Tectonophysics 744 (2018) 256–274

Contents lists available at ScienceDirect

Tectonophysics

journal homepage: www.elsevier.com/locate/tecto

Age and kinematics of the Burdur Basin: Inferences for the existence of the Fethiye Burdur Fault Zone in SW Anatolia (Turkey)

Murat Özkaptan[a], Nuretdin Kaymakci[b,*], Cor G. Langereis[c], Erhan Gülyüz[d], A. Arda Özacar[b], Bora Uzel[e], Hasan Sözbilir[e]

[a] Karadeniz Technical University, Department of Geophysical Engineering, TR-61080 Trabzon, Turkey
[b] Middle East Technical University, Geological Engineering, TR-06800 Ankara, Turkey
[c] Paleomagnetic Laboratory Fort Hoofddijk, Department of Earth Sciences, Utrecht University, Budapestlaan 17, 3584 CD Utrecht, the Netherlands
[d] Van Yüzüncü Yıl University, Department of Geological Engineering, 65080 Van, Turkey
[e] Dokuz Eylül University, Department of Geological Engineering, TR 35160 İzmir, Turkey

ARTICLE INFO

Keywords:
Burdur Basin
Fethiye-Burdur Fault Zone
Magnetostratigraphy
Anisotropy of Magnetic Susceptibility
Paleostress inversion

ABSTRACT

The Burdur Basin is a late Miocene to Pliocene fluvio-lacustrine basin in SW Anatolia. It is developed within the postulated Fethiye-Burdur Fault Zone, which was argued to be a sinistral strike-slip fault zone developed in response to propagation of the Pliny-Strabo STEP fault into SW Anatolia (Turkey). In order to assess the presence and tectonic characteristics of the fault zone, we conducted a paleomagnetic study in the Burdur basin that involved rock magnetic experiments, Anisotropy of Magnetic Susceptibility (AMS) measurements and developing a magnetostratigraphy for dating purposes. The obtained age model constrains most part of the tectonic evolution of the basin. The well exposed (~270 m thick) Burdur section revealed 3 normal and 2 reverse polarity magnetozones. We propose that the Burdur Formation spans most of the Gauss Chron (~3.4–2.5 Ma) which implies a sedimentation rate of > 18 cm/kyr. The AMS results in the section indicate NW-SE directed extension.

In addition, we have also conducted kinematic analyses from 1790 fault slip data collected at 44 sites distributed within the supposed Fethiye Burdur Fault Zone in the region. The results indicate that the region has been developed under a NW-SE directed extensional deformation regime and was dominated by NE-SW striking normal faults from late Miocene to recent. Few NW-SE striking normal faults with strike-slip components are categorized as transfer faults, which accommodated differential stretching between the Burdur and Çameli basins. Stretching amounts increase southwards demonstrating a dextral transtensional character of the transfer faults.

We have not observed any significant strike-slip motion along the NE-SW striking faults, which challenges the presence and sinistral transcurrent nature of the supposed Fethiye Burdur Fault Zone.

1. Introduction

The tectonic evolution of Western Anatolia and the Aegean region is dominated by strike-slip tectonics and extensional deformation due to the combined effort of the westwards escape of Anatolia towards the Hellenic trench (Şengör et al., 1985) and slab-edge processes at the northern edge of the northwards subducting African oceanic lithosphere (Alçiçek et al., 2005; Angelier et al., 1982; Biryol et al., 2011; Çemen and Yılmaz, 2017; Faccenna et al., 2006; Jolivet et al., 2013, 2015; van Hinsbergen et al., 2010, Özbakir et al., 2013; Wortel and Spakman, 2000). Interaction of these processes gave way to the development of a complex set of structures characterized by strike-slip faults, mainly in northern and central Anatolia, while western Anatolia and the Aegean region is dominated by normal faults striking in various directions. The tectonic position of SW Anatolia has been subject to debate since the late 1970's. It is located at the junction of Pliny-Strabo and Cyprian trenches where they meet and make very sharp southwards bends. Recent mantle tomographic images (Biryol et al., 2011; Faccenna et al., 2006; Govers and Wortel, 2005; van Hinsbergen et al., 2010; Portner et al., 2018; Wortel and Spakman, 2000) indicate that the northern edge of the subducted African slab is torn and produced a mantle window below western Anatolia, while the Pliny-Strabo Trench is a STEP fault (sensu Govers and Wortel, 2005) which accommodated asymmetric retreat of the Hellenic trench (Duermeijer et al., 2000; Özbakir et al., 2013; Kaymakci et al., 2018).

Dumont et al. (1979) were among the pioneers who recognized the

* Corresponding author.
E-mail address: kaymakci@metu.edu.tr (N. Kaymakci).

https://doi.org/10.1016/j.tecto.2018.07.009
Received 28 February 2018; Received in revised form 6 July 2018; Accepted 10 July 2018

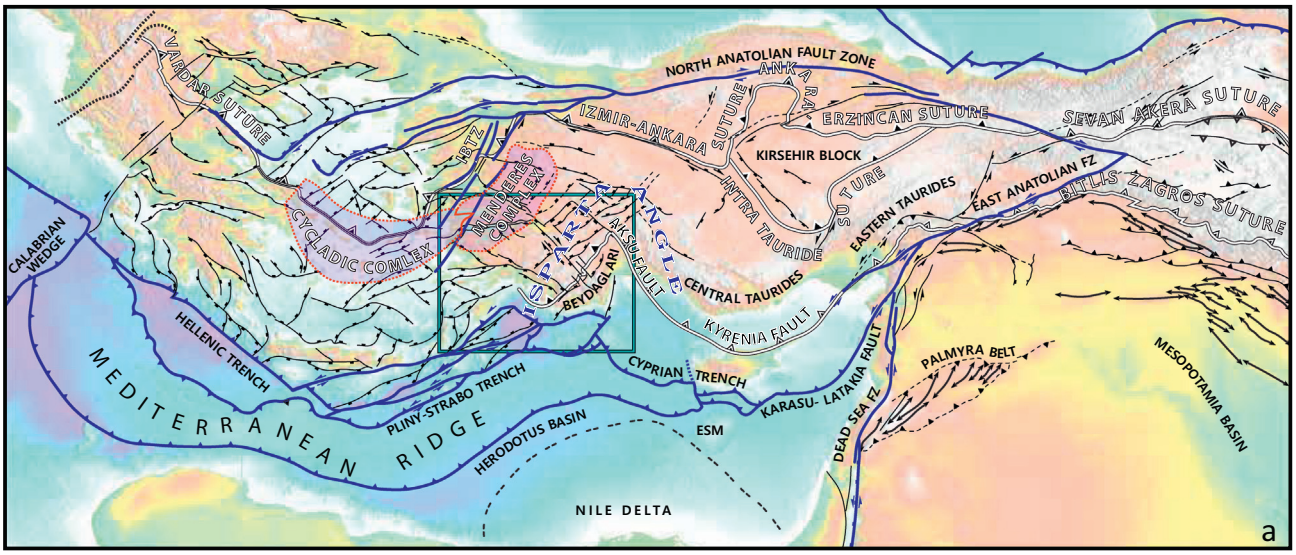

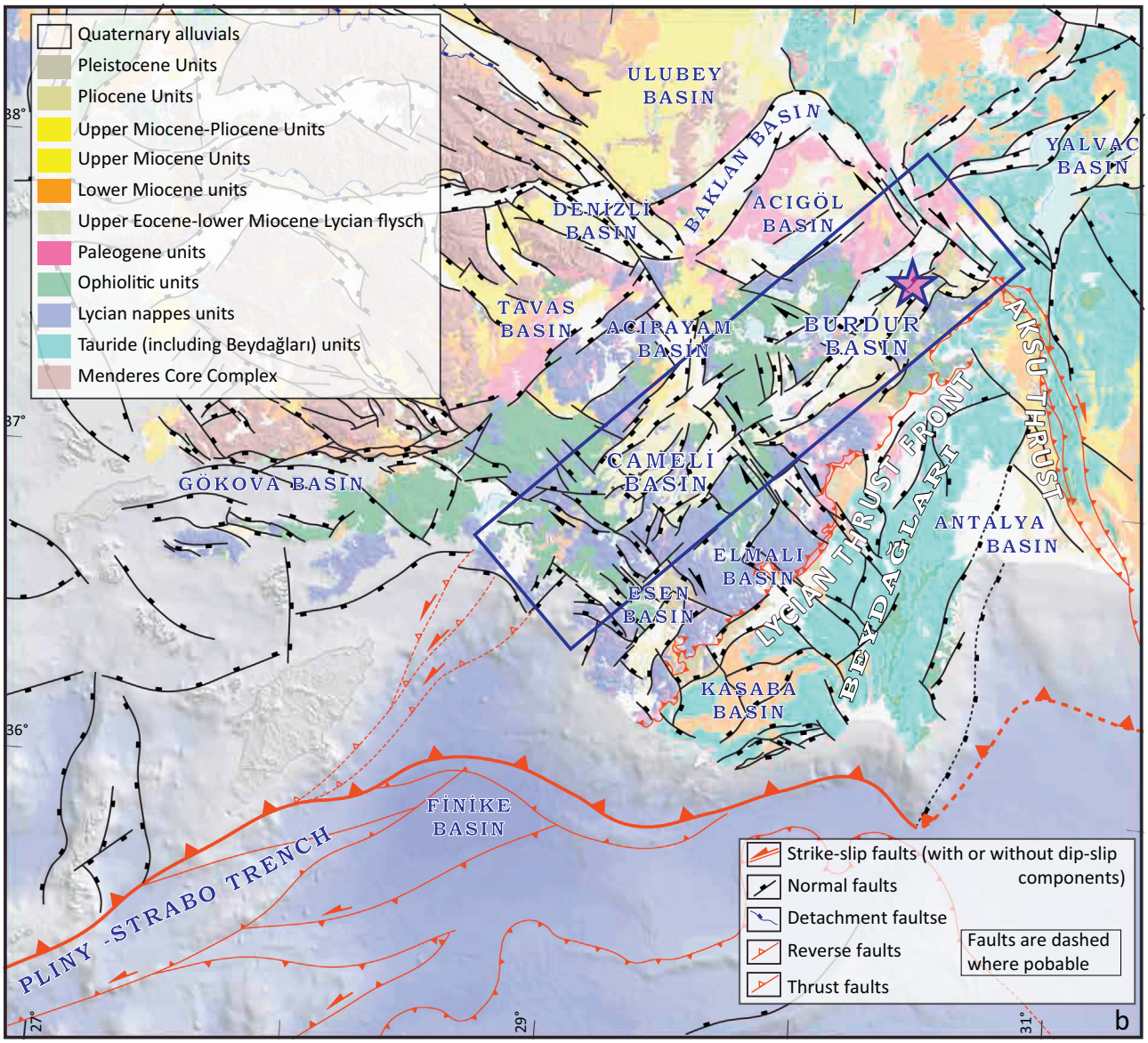

Fig. 1. a) Tectonic scheme of Eastern Mediterranean region depicting major presently active fault systems and paleotectonic tectonic blocks and suture zones. b) Simplified geological map of SW Anatolia. Rectangle indicates the Study Area and the star is the location of Magnetostratigraphical section. İBTZ: İzmir-Balıkesir Transfer Zone; ESM: Eratosthenes Sea Mount (Aksu et al., 2005; Kaymakci et al., 2010, 2018; Ocakoğlu, 2012; Uzel et al., 2013, 2015).

role of slab edge processes on the overriding plate and they proposed that the Fethiye Budur Fault zone (FBFZ) is its manifestation. They claimed that the FBFZ is a sinistral strike-slip fault zone extending from Fethiye to the northern edge of the Isparta Angle (Fig. 1). Recently, the issue became a topic of debate and a number of studies have been published. Some authors (Hall et al., 2014; Elitez et al., 2015, 2016, 2017) argue that the Fethiye-Burdur Fault Zone is the northwards continuation of the Pliny-Strabo STEP fault into SW Anatolia. It is not a single fault zone but distributed over a very broad area reaching up to 80 km. They named the zone as the Fethiye Burdur Shear Zone (Hall et al., 2014). On the other hand, Kaymakci et al. (2014, 2017, 2018), Özkaptan et al. (2014), Alçiçek (2015) and Alçiçek et al. (2017) questioned the existence of such a sinistral strike-slip fault zone in the region.

In this regard, the main purpose of this study is to evaluate the characteristics, kinematic properties and tectonic styles of the presumed Fethiye-Burdur Fault Zone and to constrain its commencement age and exact timing by means of data obtained in the field. For this purpose we have conducted a very rigorous fault kinematic analysis based on fault slip data sets collected from the fault zone and we used paleomagnetic tools to constrain the age of fluvio-lacustrine sequences in the Burdur Basin. We also conducted an Anisotropy of Magnetic Susceptibility (AMS) study on the paleomagnetic samples to constrain principal strain directions in the basin that, combined with fault slip data, provide valuable information about the regional deformation patterns and tectonic regime that prevailed during and after the deposition of the basin infill. The obtained information is used to assess the presence and kinematics of the presumed Fethiye Burdur Fault Zone, and its possible link with the Pliny-Strabo Trench.

1.1. Regional geological setting

The Late Paleogene to Early Neogene tectonic development of SW Anatolia is related to emplacement of the Lycian Nappes over the Beydağları Platform during the Eocene-Middle Miocene interval (Hayward, 1984a), together with Neotethyan ophiolitic nappes, which are thought to originate from the oceanic domain demarcated by the İzmir-Ankara Suture Zone located north of the Menderes Massif. The Lycian Nappes originated from a basin located between the Menderes Massif and the Beydağları Platform, namely the Kızılca Basin, both of which imbricated and collectively thrusted over the Beydağları Platform (Poisson, 1984). This gave way to the development of the Lycian foreland basins in front of the eastwards advancing nappe stacks, such as the Kasaba and Elmalı basins (Fig. 1).

Thrusting and emplacement of the Lycian Nappes continued until the end of the Serravallian (Hayward, 1984a,b). Subsequently, the region was subjected to extensional deformation due to rollback and retreat of northwards subducting African oceanic lithosphere along the Hellenic trench (Angelier et al., 1982, Faccenna et al., 2006; Le Pichon and Angelier, 1979; van Hinsbergen et al., 2010). Although the region is dominated by extensional deformation since early Miocene, thrusting and compressional deformation prevailed within the Isparta Angle, until recently (Koç et al., 2016a). The Isparta Angle is a triangular zone; its eastern flank is defined by the central Tauride block and its western flank by the Beydağları Platform. Its outer rim is characterized mainly by normal fault controlled basins such as the Burdur and Çameli basins (Alçiçek et al., 2013a) and therefore dominated by extensional deformation, while its internal part is dominated by compressional deformation exerted by the Aksu Fault (Akay and Uysal, 1988; Flecker et al., 1998; Sözbilir, 2005; Alçiçek et al., 2005, 2006, 2013a,b; Alçiçek, 2007; Çiner et al., 2008; Üner et al., 2015; Elitez and Yaltırak, 2016; Koç et al., 2016a). Marine conditions continued up to the Pliocene especially in the Aksu Basin (Çiner et al., 2008; Koç et al., 2016a,b, 2012; Monod et al., 2006) and the marine to continental transition in the western flank of the Isparta Angle is associated with the basins related to the emplacement of the Lycian Nappes and are developed as piggy-back basins on the eastwards advancing nappes during the Middle Miocene (Alçiçek, 2007; Alçiçek et al., 2006, 2012; Alçiçek and ten Veen, 2008; Sözbilir, 2005; ten Veen et al., 2009; Verhaert et al., 2006). The timing and extent of marine deposition as well as timing of the change from the compressional tectonic regime related to Lycian Nappe emplacement to the presently active extensional tectonic regime is still under debate, owing to the scarcity of tectono-stratigraphical studies and precise dating of continental units in the region. However, recent studies addressing this issue provide valuable information about the age and depositional conditions of sedimentary units (Alçiçek et al., 2016, 2018). Dating of continental units, in these studies, are based on micromammal fauna and radiometric data belonging to the intercalated and intruding magmatic rocks. Unfortunately, most of these data are limited to only some of the basins and their correlation with adjacent basins. Only the Çameli Basin provided a precise stratigraphy (Alçiçek et al., 2005). Apart from this study, age dating in the region is based mostly on spot sampling distributed in various stratigraphical sequences or on long distance correlations.

2. Burdur Basin

The NE-SW striking Burdur Basin is a half graben developed along the northwestern limb of the Isparta Angle. It is located within the Fethiye Burdur Fault Zone and developed during the Late Miocene to Recent (Price, 1989; Price and Scott, 1991), which puts it in a unique position in terms of unraveling the age and deformation styles of Fethiye-Burdur Fault Zone.

The basement units of the basin are composed of various lithostratigraphical units of the Lycian Nappes that comprise Mesozoic carbonates, late Cretaceous ophiolitic mélanges and ultramafic rocks belonging to Neotethys Ocean, Paleocene to Eocene neritic carbonates deposited on top of the ophiolitic and other Mesozoic units. All of these units are emplaced on top of the Beydağları Platform, by an intervening middle Eocene to Middle Miocene flysch units that acted as a decollement level and were deposited in the foreland basin in front of the eastwards advancing Lycian Nappes (Flecker et al., 1998, 2005; Hayward, 1984b; Konak and Şenel, 2002; Alçiçek et al., 2013a; Piper et al., 2002; Price and Scott, 1994; Robertson et al., 2003; Şenel, 1997, 2002; Sözbilir, 2005; Üner et al., 2015; Uysal et al., 1980; Waldron, 1984; Nemec et al., 2018) (Fig. 2).

The infill of the Burdur Basin is exposed over large areas and comprises the late Miocene to Pliocene Burdur Formation. It reaches up to 1100 m of stratigraphic thickness. The formation is represented by three depositional settings; (i) it starts at the bottom with alluvial fan and fluvial deposits, (ii) it grades upwards into lacustrine facies and finally (iii) ends with a fluvio-deltaic facies. These depositional settings correspond to the Çendik, Akdere and Günalan members (Price, 1989) which are intercalated with the Gölcük volcanics (Fig. 3).

The Çendik Member is the oldest stratigraphic succession of the Burdur Formation and unconformably overlies basement units that comprise middle Eocene to Middle Miocene flysch to molasse sequences, Mesozoic to Eocene limestones and intercalated clastics, ophiolitic units including ultramafic rocks, radiolarian cherts, various pelagic units, and tectonic blocks derived from various lithologies of the Lycian Nappes. The member shows a dominantly fluvial character and laterally grades into alluvial fan deposits that developed at the basin margins along the basin bounding faults. The oldest age for this unit has been based on an Astragalus belonging? to a *Giraffidae* sp. indicating a Turolian age (9–5.3 Ma as reported by Price (1989)).

The Akdere Member is represented by a ~600 m thick sequence exposed over large areas and has a lacustrine facies. The member can easily be distinguished from other units by its light cream, pale-beige color, well bedded sandstone-mudstone-claystone-marl alternations and minor intercalations of gypsum. Layers of tuff belonging to older successions of the Gölcük volcanics (4.7 ± 0.2 to 4.0 ± 0.2 Ma dated by K/Ar, Lefevre et al., 1983) are also found within the member

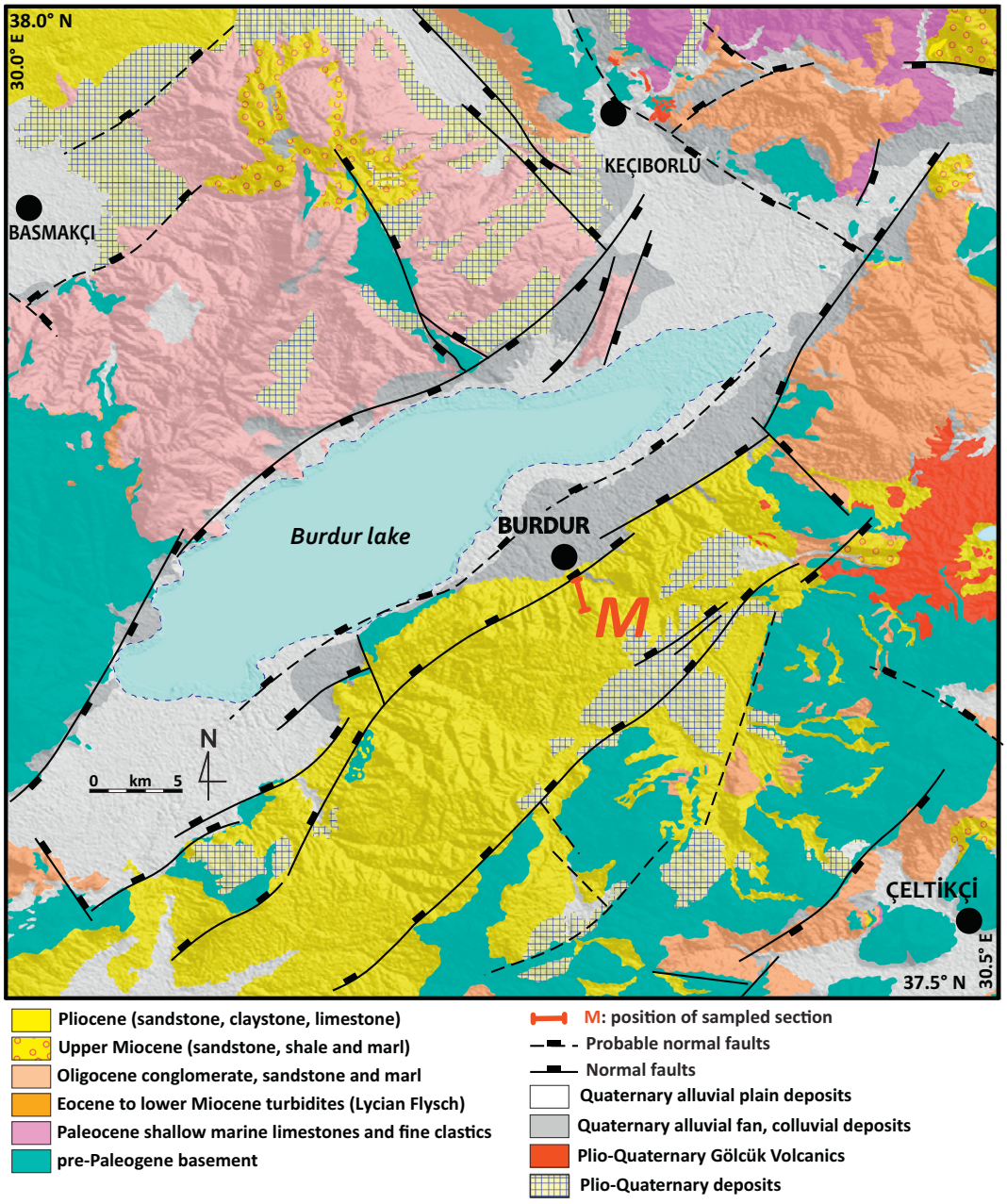

Fig. 2. Geological map of the Burdur Basin (Şenel, 1997; Şenel et al., 1994).

(Alçiçek et al., 2013a; Bozcu et al., 2007; Yalçınkaya et al., 1986). Recent fossil vertebrate findings in the lacustrine succession of the Akdere Member indicate a Ruscinian age at the base and a Villanyian age at the top and confirm those previous age determinations (Alçiçek et al., 2013a,b).

The Günalan Member is the youngest member of the Burdur Formation (Price, 1989). It overlies the Akdere Member with a local intra-formational (low angle) angular unconformity. According to Price and Scott (1991), this local unconformity is the result of differential rotation of the underlying normal fault block. It is composed dominantly of alluvial fan and related fluvial successions comprising conglomerate, sandstone and mudstone accumulated along the northwest facing normal faults bounding the basin in the SE. It is unconformably overlain by the younger levels of the Gölcük volcanics dated from ~200 ka to 24 ± 2 ka (Platevoet et al., 2008) and Quaternary alluvial deposits. According to Alçiçek et al. (2013b) the Günalan Member abounds in large mammal fossil remains. The complete list of fossils and their corresponding age ranges are presented in (Alçiçek et al., 2017, 2018).

The age of Burdur Formation is still debated among various researchers. The Akdere Member includes fauna comprising various palynomorphs and ostracodes, indicating an early Pliocene to early Pleistocene age (Bering, 1971). Karaman (1986) proposed a Pliocene age for the Burdur Formation based on palynomorphs obtained from lignite levels in the Günalan Member (Karaman, 1986). Based on macromammal fauna from the Çendik Member and ostracode fauna from the Akdere Member, Price (1989) argued that deposition of the formation commenced in the late Miocene and continued up to the Pliocene.

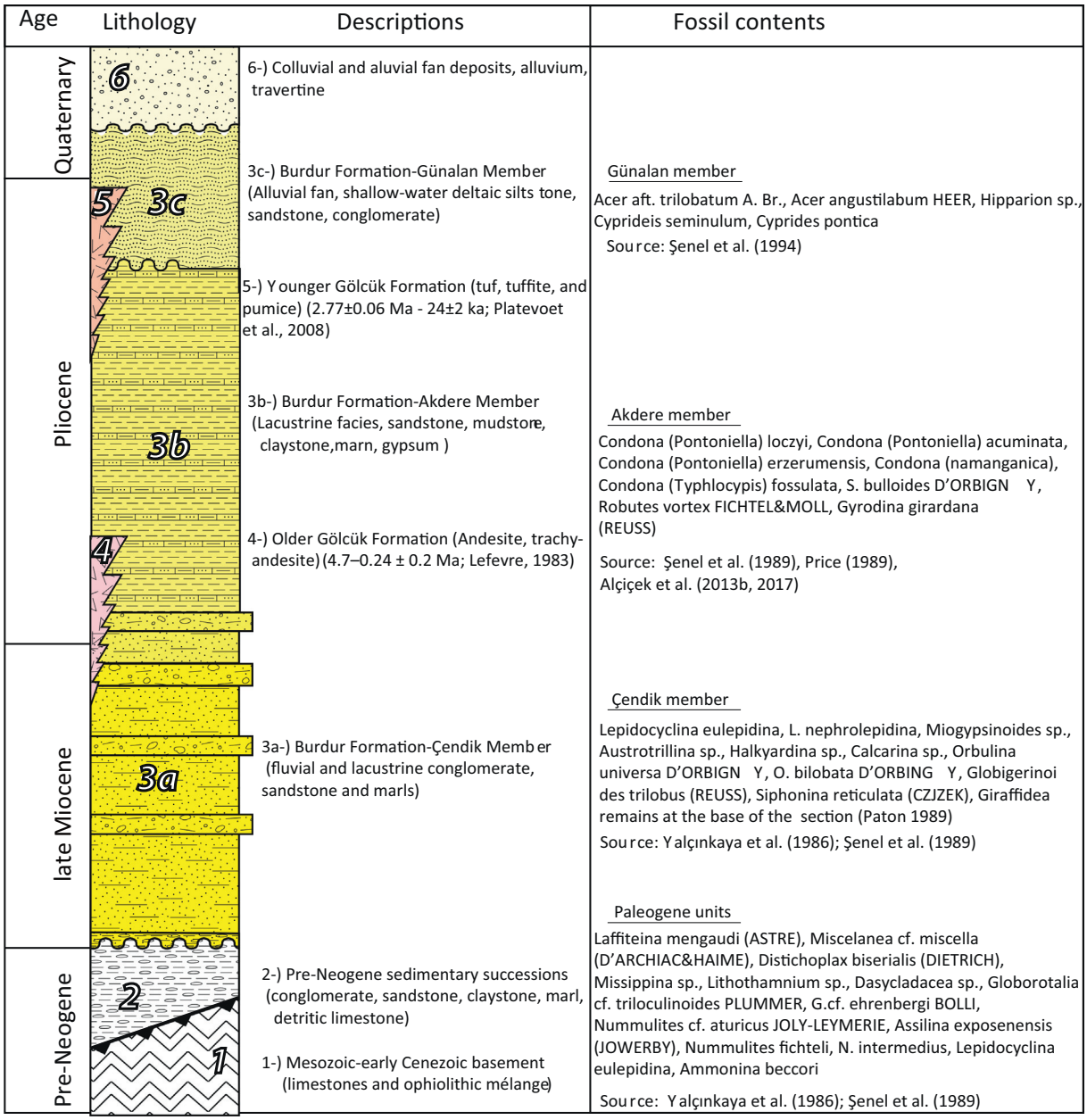

Fig. 3. Generalized stratigraphic section of the Burdur Basin (Karaman, 1986; Price, 1989; Bozcu et al., 2007; Şenel et al., 1994; Alçiçek et al., 2013a,b, 2017, 2018).

3. Methods and results

3.1. Sampling

In total, a stratigraphic thickness of 267.5 m of the Burdur Formation has been sampled for paleomagnetic analyses that include magnetostratigraphy, AMS and thermomagnetic experiments. Standard core samples (Ø 25 mm) were collected in the field using a portable gasoline-powered water-cooled drilling machine for well-lithified layers. For less consolidated or weak layers an electrical drill was preferred. At least two but generally three oriented cores were collected at each of the 94 stratigraphic levels, yielding on average a 2–3 m stratigraphic resolution. The samples were taken from fresh and fine-grained levels from an alternation of white to yellowish siltstone-mudstone and marl, intercalated with sandstones (Figs. 4 and 7). Orientation of the cores and bedding attitudes were measured with a magnetic compass throughout the section. All compass readings were corrected for the declination at the time of sampling (4.85°E). Bedding planes are nearly horizontal and vary around 160/08° (dip direction/dip) throughout the section.

3.2. Demagnetization

All oriented cores were cut into standard paleomagnetic specimens (22 mm) in the paleomagnetic laboratory Fort Hoofddijk at Utrecht University. The magnetic remanence of the specimens was investigated by thermal (TH) and alternating field (AF) demagnetization. At least two specimens for each stratigraphic level were demagnetized, one treated thermally and one by alternating fields. Thermal demagnetization was applied on 82 specimens using 10–20 °C steps, from room temperature up to 300–350 °C depending on the maximum unblocking temperature, in a magnetically shielded ASC furnace (Model TD48-SC), which has a residual field < 10 nT. Before AF demagnetization, specimens were heated to 150 °C to remove a viscous remanent magnetization (VRM) and possible stress in magnetite grains by low temperature oxidation (Gong et al., 2008; Van Velzen and Zijderveld, 1995). AF

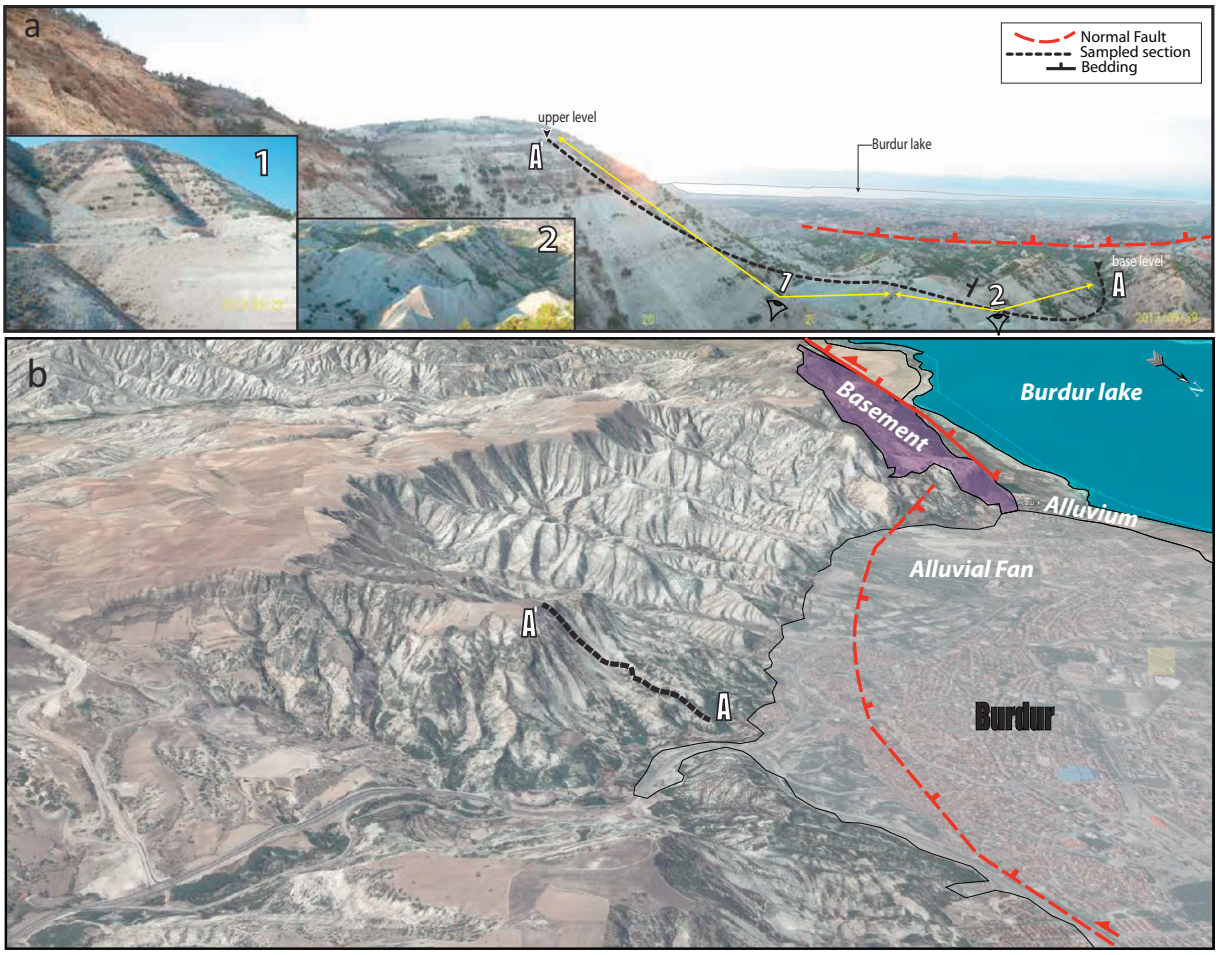

Fig. 4. a) Magnetostratigraphic sampling section of the Burdur Formation. A–A′ is the path followed for sampling in the field. Inset field photos 1 and 2 depict top and bottom levels of the section, respectively. b) GoogleEarth image showing general view of the section.

demagnetization was carried out by using an in-house developed robot assisted and fully automated system (Mullender et al., 2016) attached to a horizontal pass-through 2G Enterprises DC SQUID cryogenic magnetometer (noise level 1–2 × 10^{-12} Am^2) in a magnetically shielded room (residual field < 200 nT). After heating to 150 °C, the AF demagnetization was performed by increments of 2–6 mT, up to a maximum of 50 mT. Hence, we obtained at least two remanent magnetization results for each level to compare their directions and improve the magnetostratigraphic resolution from the Burdur section.

Stepwise demagnetization diagrams of the NRM results were analyzed using orthogonal vector diagrams (Zijderveld, 1967). Representative examples for three different stratigraphic levels are shown in Fig. 5(a1–a2, b1–2, and c1–c2). The characteristic remanent magnetization (ChRM) directions were calculated by taking generally four to seven successive TH or AF steps following the eigenvector approach of (Kirschvink, 1980) in the majority of the specimens. In a limited number of case, we had to use a great-circle approach (McFadden and McElhinny, 1988) because secondary magnetization(s) could not be entirely separated from the original magnetization (Fig. 5, a1 and b2). The method utilizes well-determined directions (setpoints) to calculate best-fit directions on the great circle. We calculated Fisher (1953) site means distributions for normal and reversed polarity results separately, and we used the statistical criteria of Deenen et al. (2011). We applied a fixed 45° cut-off on the corresponding VGP distributions, while errors in declinations (ΔD_x) and inclinations (ΔI_x) were calculated from A95 (the 95% cone of confidence of VGPs) following (Butler, 1992). All interpretations and statistical procedures were done using the on-line portal of *Paleomagnetism.org* (Koymans et al., 2016).

3.3. Rock magnetism

To determine the magnetic carrier(s) of the samples from various lithologies, we applied thermomagnetic runs on selected samples, using a modified horizontal translation type Curie balance, with a sensitivity of ~5 × 10^{-9} Am^2 (Mullender et al., 1993). Approximately 0.3–0.9 g of powdered rock sample (depending on the magnetic intensity of the sample) was put into a quartz-glass sample holder and measured using heating-cooling cycles (with rates of 10 °C/min.) up to successively higher temperatures (max. 700 °C). Based on the thermomagnetic curves, Curie temperatures were determined following Fabian et al. (2013).

Thermomagnetic runs of 11 different levels from clay-mud-sandstone lithologies in the Burdur Formation were done. Three examples are shown in Fig. 5, and show initial magnetization intensities ranging 0.5–4.0 × 10^{-7} Am^2, The other 8 results are given in the supplementary information. The light colored claystones show a typical paramagnetic behaviour, indicating that the thermomagnetic curve is mostly/entirely determined by the (paramagnetic) clay content. The darker lithologies with a sandy-muddy claystone composition show the typical transition of pyrite to fine-grained magnetite starting at 390–420 °C, causing an increase of the magnetization up to 500 °C followed by a decrease due to the demagnetization/oxidation of the newly formed magnetite at ~550 °C (Passier et al., 2001). The Curie balance curves therefore suggest that iron sulfides (pyrite, but likely including greigite as the major remanence carrier) constitute an important part of the magnetic minerals present. The newly formed magnetite dominates the demagnetization behaviour at temperatures

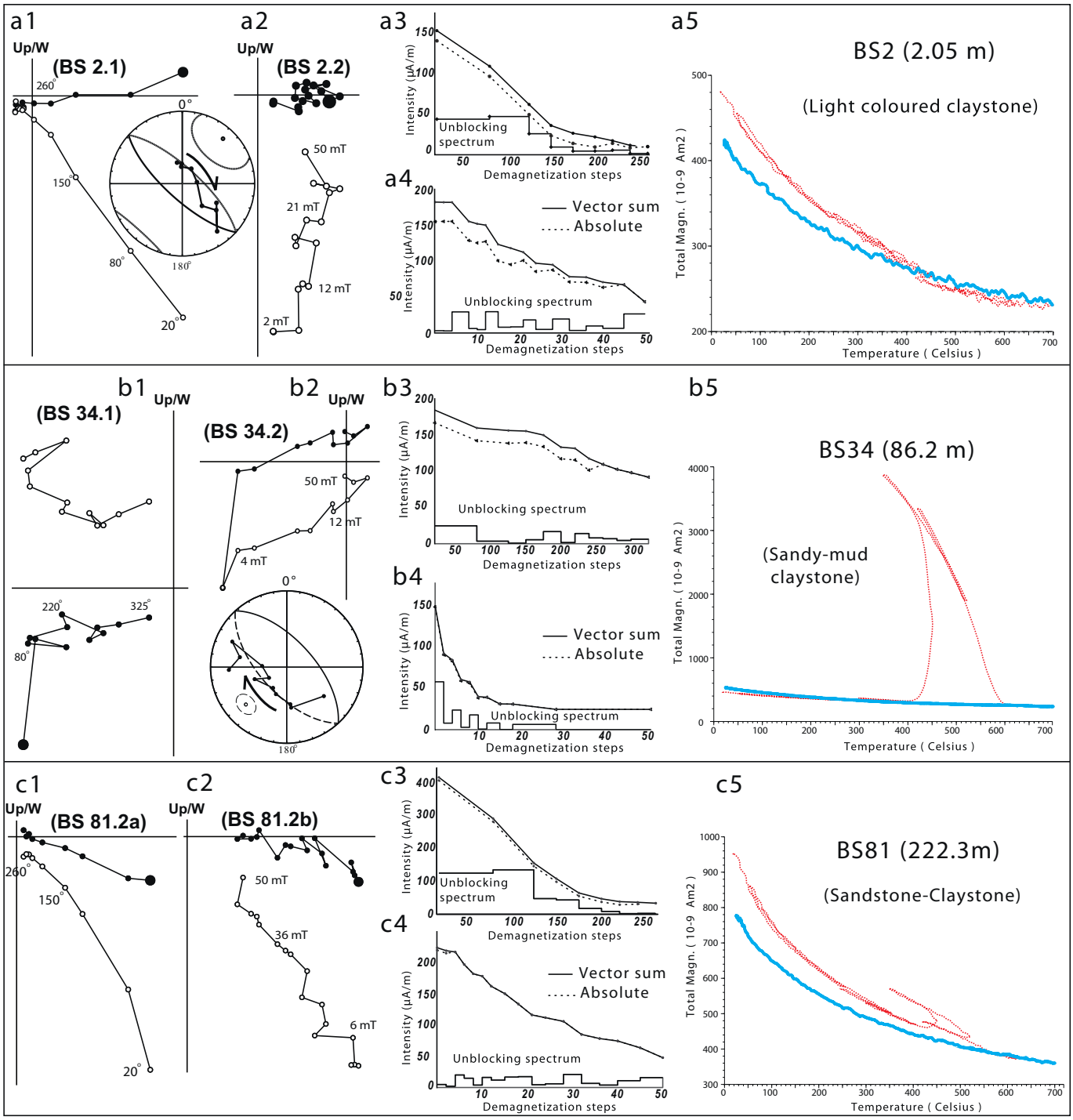

Fig. 5. Zijderveld diagrams (Zijderveld, 1967) of representative samples demagnetized using thermal (TH) and alternating field (AF) demagnetization shown tectonic (TC) coordinates (left). The solid and open dots represent projections on the horizontal and vertical planes, respectively. Demagnetization step values are in °C or in mT shown for both AF&TH at middle. Thermomagnetic (curie-balance) curves (right) generated with stepwise heating protocol (Mullender et al., 1993) for three representative samples in different levels from the Burdur Formation. Great circle plots a1 and b2, are the lower hemisphere equal area projection plots of demagnetization values developed by McFadden and McElhinny (1988).

above 400 °C and causes spurious magnetizations. For this reason, thermal demagnetization could only be done to 350–400 °C, while AF demagnetization is done up to ~50 mT since at higher fields a gyroremanent magnetization is acquired (Dankers and Zijderveld, 1981), which is typical of greigite.

3.4. Anisotropy of Magnetic Susceptibility (AMS)

The AMS was measured to determine the origin of the magnetic fabric, whether it is a purely sedimentary fabric acquired during deposition (k_{min} vertical to bedding plane, k_{int}, k_{max} randomly distributed)

Table 1
a) Anisotropy of Magnetic Susceptibility (AMS) parameters from the magnetostratigraphic section of Burdur locality. b) Site mean normal/reverse, and reversed polarity paleomagnetic results from the same site.

a)	N_{AMS}	Bedding	$k_m * 10^{-6}$(SI)	L	F	Pj	T	D/I (k_{max})	D/I (k_{min})	e_1	e_2	e_3
		Azi/dip										
In situ	114	090/08062/10	49.8	1.002	1.017	1.021	0.751	110.9/10.4	308.7/79.1	54.3/9.5	54.3/14.8	15.2/9.7
Tilt corrected	114		49.8	1.002	1.017	1.021	0.751	111.6/3.7	246.7/84.8	54.5/9.9	54.6/14.7	15.1/10.0

b)	N_s	N_{45}	D	ΔDx	I	ΔIx	k	α95	K	A95	A95min	A95max
ChRM directions (in situ)												
Normal	84	82	359.2	3.6	53.2	3.1	43.6	2.4	28.2	3.0	2.1	5.1
Reversed	14	13	157.6	11.7	−49.9	11.3	23.5	8.7	17.9	10.1	4.3	16.3
N + R	98	94	357.9	3.6	52.8	3.1	37.2	2.4	24.7	3.0	1.9	4.7
ChRM directions (tilt corrected)												
Normal	84	82	3.1	4.6	61.3	2.9	43.6	2.4	22.4	3.4	2.1	5.1
Reversed	14	13	156.1	14.7	−58.3	10.4	23.5	8.7	14.2	11.4	4.3	16.3
N + R	98	94	1.4	4.5	61	2.9	37.2	2.4	19.8	3.4	1.9	4.7

a) Geographic coordinates use WGS84 datum. Start point = 37.707120°N, 30.292550°E and end point = 37.701368°N, 30.293683°E. N_{AMS}, number of studied samples at location. k_m, mean susceptibility in 10^{-4} SI. Magnetic lineation (L), magnetic foliation (F), corrected anisotropy degree (Pj), and shape factor (T) according to Jelínek (1978). D and I are the mean declination and inclination of the maximum and minimum susceptibility axis, respectively. e1, e2, and e3 semi-angle of the 95% confidence ellipse around the declination/inclination of the mean maximum, intermediate, and minimum susceptibility axes, respectively. Declination of the mean lineation. b) Ns/N45 number of specimens from which a direction has been interpreted/number of specimens after application of a 45° fixed cut-off on the VGPs, D: declination, I: inclination, ΔDx: declination error, ΔIx: inclination error, k: estimate of the precision parameter determined from the ChRM directions, a95: cone of confidence determined from the ChRM directions, K: precision parameter determined from the mean virtual geomagnetic pole (VGP) direction, A95: cone of confidence determined from the mean VGP direction, A95min and A95max correspond to the confidence envelope of Deenen et al. (2011, 2014).

or a tectonic fabric due to tectonic deformation after deposition (causing clustering of k_{int}, k_{max}). In sediments, the paleocurrent during the transportation may control the AMS tensor, but only in high-energy sedimentary environments. In the case of fine-grained sediments such as the mudstones and marls in our study, the anisotropy is therefore most likely related to post depositional deformation. Therefore, the magnetic fabric orientations obtained from the AMS measurements can be used for unraveling the deformation history of the sedimentary basins (Borradaile and Tarling, 1981; Cifelli et al., 2004a,b, 2005, 2007; Graham, 1966; Kissel et al., 1986; Sagnotti et al., 1994; Soto et al., 2007). The AMS tensor can be described as an ellipsoid with three principal susceptibility vectors $k_{max} \geq k_{int} \geq k_{min}$ (Hrouda, 1982). In case of a tectonically induced AMS ellipsoid, the susceptibility vectors correspond to the principal strain axes, with k_{min} being perpendicular to bedding and k_{max} parallel to extension or, equivalently, perpendicular to compression (Duermeijer et al., 1998). The low field magnetic susceptibility measurements were carried out with the AGICO Multi-Function Kappabridge (MFK1-FA), having a sensitivity level of 2×10^{-8} SI.

The AMS (in-situ and tilt corrected) ellipsoids and related parameters were evaluated using Jelinek statistics (Jelínek, 1977, 1978), and the results (Table 1a) are illustrated in Fig. 6. Mean susceptibilities (k_m) range 10–200 $\times 10^{-6}$ SI and cluster around 50–100 $\times 10^{-6}$ SI. The plot of k_m versus stratigraphic level (Fig. 7), shows several intervals with distinctly higher values, up to 200 $\times 10^{-6}$ SI, between 60 and 80, 110–120 and 215–230 m. The high susceptibility results tend to be from the dark mudstones. The corrected anisotropy degree Pj varies between 1.02 and 1.078 with an average of ~1.04, indicating that the magnetic fabric of the studied stratigraphy has been affected by a low but distinct degree of anisotropy. The k_m versus Pj graph (Fig. 6e) implies that the anisotropy varies independently from the quantity of magnetic minerals in the matrix, but there is some correlation of the shape factor (T) versus Pj (Fig. 6f) possibly due to strain effects related to tectonic deformation.

The AMS ellipsoid is well defined, with a small confidence ellipse for k_{min}, while k_{int} and k_{max} have larger confidence ellipses that show a small overlap. The T values (up to ~0.95) characterize a strong oblate geometry, except for some of the specimens which have negative T values down to −0.3 (prolate). Mean k_{min} is near vertical but slightly tilted in geographic coordinates (in-situ). Upon tilt correction, k_{min} is perpendicular to the bedding plane within error, while k_{int} and k_{max} axes tend to be parallel to the bedding plane (Fig. 6a–d) and show distinct clusters, in NE-SW and NW-SE direction, respectively. This is typical for compacted and weakly deformed sedimentary rocks (e.g., Borradaile, 1987; Borradaile and Jackson, 2004; Cifelli et al., 2005; Duermeijer et al., 1998; Mattei et al., 1997, 1999). The k_{max} directions are scattered but have a mean distinctly different from that of k_{int}. Both in-situ and tilt corrected k_{max} mean directions have an azimuth of 110°N which is nearly parallel to the general dip direction of the strata (Fig. 6). The mean k_{int} directions have a mean azimuth of 020°N.

4. Paleomagnetic analysis

4.1. Vertical axis rotation

Equal area projection of ChRM directions are shown in Fig. 8, the detailed statistical results are given in Table 1b. Among the analyzed 175 specimens, only 98 of them produced interpretable results while the remaining 77 specimens are excluded from further interpretations, since they had very low intensities close to the sensitivity of the magnetometer after a few demagnetization steps, showed random 'impossible' directions or interpretation was simply not possible. The majority of the reliable data indicate normal polarity directions of our Burdur section (86%). The intensities of the specimens range between 16 and 850 μA/m (Fig. 7). The mean of the normal directions have a declination (D) of 357.9° ± 3.6° (in situ) and 1.4° ± 4.5° (tilt corrected). The ChRM distributions before and after tilt correction show a statistically similar scatter before (K = 24.7, A95 = 3) and after tilt correction (K = 19.8, A95 = 3.4). Upon tilt correction the mean inclination increases from 58.2° ± 3.1° to 61.0° ± 2.9° (Fig. 8 and Table 1b). This suggests that a recent overprint has not been fully removed. The distribution of the reverse polarity directions displays a slightly higher scatter both before and after tilt corrections (K = 17.9, A95 = 10.1, and K = 14.2, A95 = 11.4, respectively). The ChRM

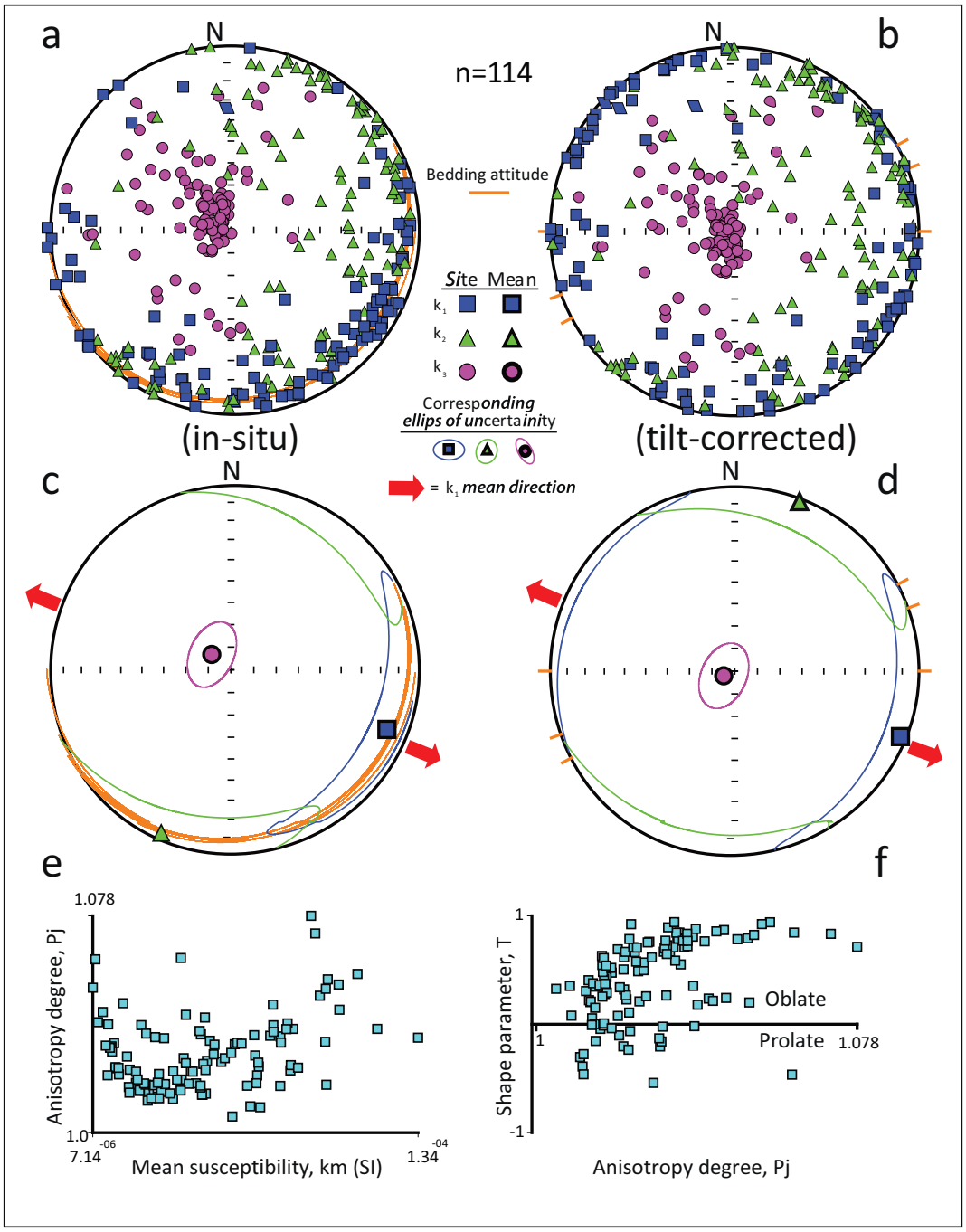

Fig. 6. a) Lower hemisphere, equal-area projection of in situ, b) tilt corrected AMS principal magnetofabric vectors, c–d) indicate their mean values (larger symbols) and red arrow indicate horizontal component of mean maximum anisotropy direction. e) Anisotropy degree versus mean susceptibility, and f) shape vector versus corrected anisotropy degree diagram. (For interpretation of the references to color in this figure legend, the reader is referred to the web version of this article.)

directions determined from reverse polarities indicate counterclockwise (CCW) rotation, D = 157.6° (−22.4°) ± 11.7° and D = 156.1° (−23.9°) ± 14.7° before and after tilt correction, respectively. The mean normal directions indicate no significant rotation after tilt correction, which may be caused by an unremoved or unrecognized overprint. Since a normal overprint is more easily recognized in reversed samples, this may explain the discrepancy between normal and reverse polarity means. Indeed, the reversal test is negative. By averaging the results of both normal and reverse polarity specimens (Ns = 98) this unremoved overprint is largely nullified (e.g. Scheepers and Langereis, 1993), although N of the normal samples is larger than that of the reversed samples. This results in no significant rotation ([360°–357.9° =] 2.1° ± 3.6°) before and (1.4° ± 4.5°) after tilt correction.

4.2. Magnetostratigraphy

In Fig. 7, initial intensity and mean magnetic susceptibility are plotted with respect to the stratigraphy. The magnetic properties present low to moderate initial intensities that rapidly decrease until 150 °C, and then slowly decrease until 250–275 °C but with generally very low intensities around 50 μA/m or less (Fig. 5, a3–a4, c3–c4). The mean magnetic susceptibilities vary within 50–150 $*10^{-6}$ (SI) range (Fig. 7). In general, initial intensities are low (100–300 μA/m) and are

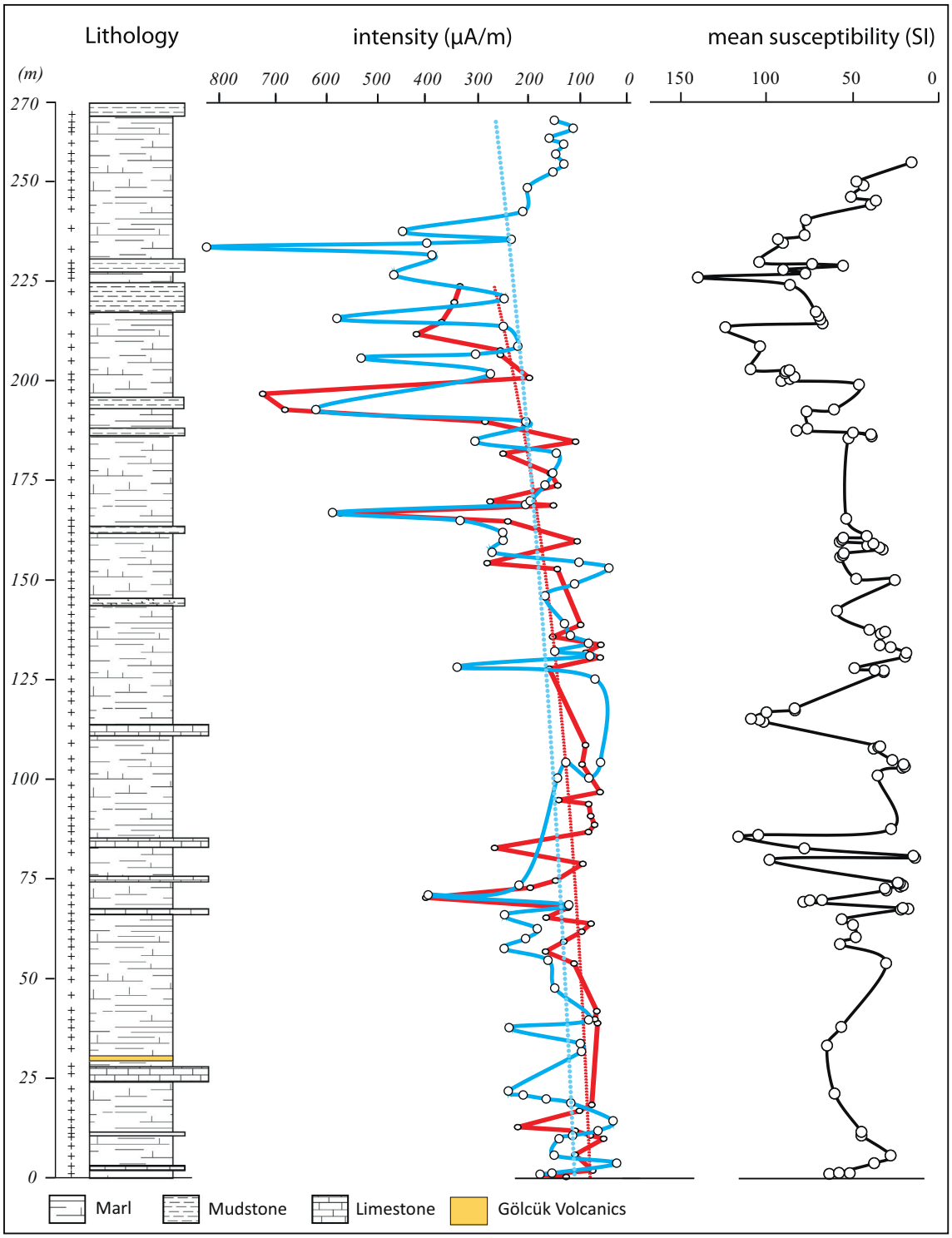

Fig. 7. Lithological log of the succession versus declination, inclination, magnetic intensity and mean susceptibility. Plus signs (+) represent the sampled levels, blue and red lines correspond to Alternating Field (AF) and Thermal (TH) demagnetization results. (For interpretation of the references to color in this figure legend, the reader is referred to the web version of this article.)

slightly higher in the upper part of the section (300–600 μA/m), but decrease sharply again in the uppermost part (100–300 μA/m). The mean susceptibility (Fig. 7) shows an alternation of intervals of low ($50 * 10^{-6}$) and relatively higher ($150 * 10^{-6}$) values.

The magnetostratigraphic results indicate two reversed and three normal polarity intervals that we consider to be reliable (Fig. 9). The samples from both the lowermost and uppermost parts of the section (0–52 m and above 225 m, respectively levels) did not produce reliable results, therefore we did not include these results in our interpretations; these intervals are indicated with grey shading.

5. Paleostress analysis

In order to reconstruct paleostress configurations in the region1836 fault slip data have been collected from 44 sites distributed throughout the Burdur and Çameli basins. Among these, only 2.5% (46) were found

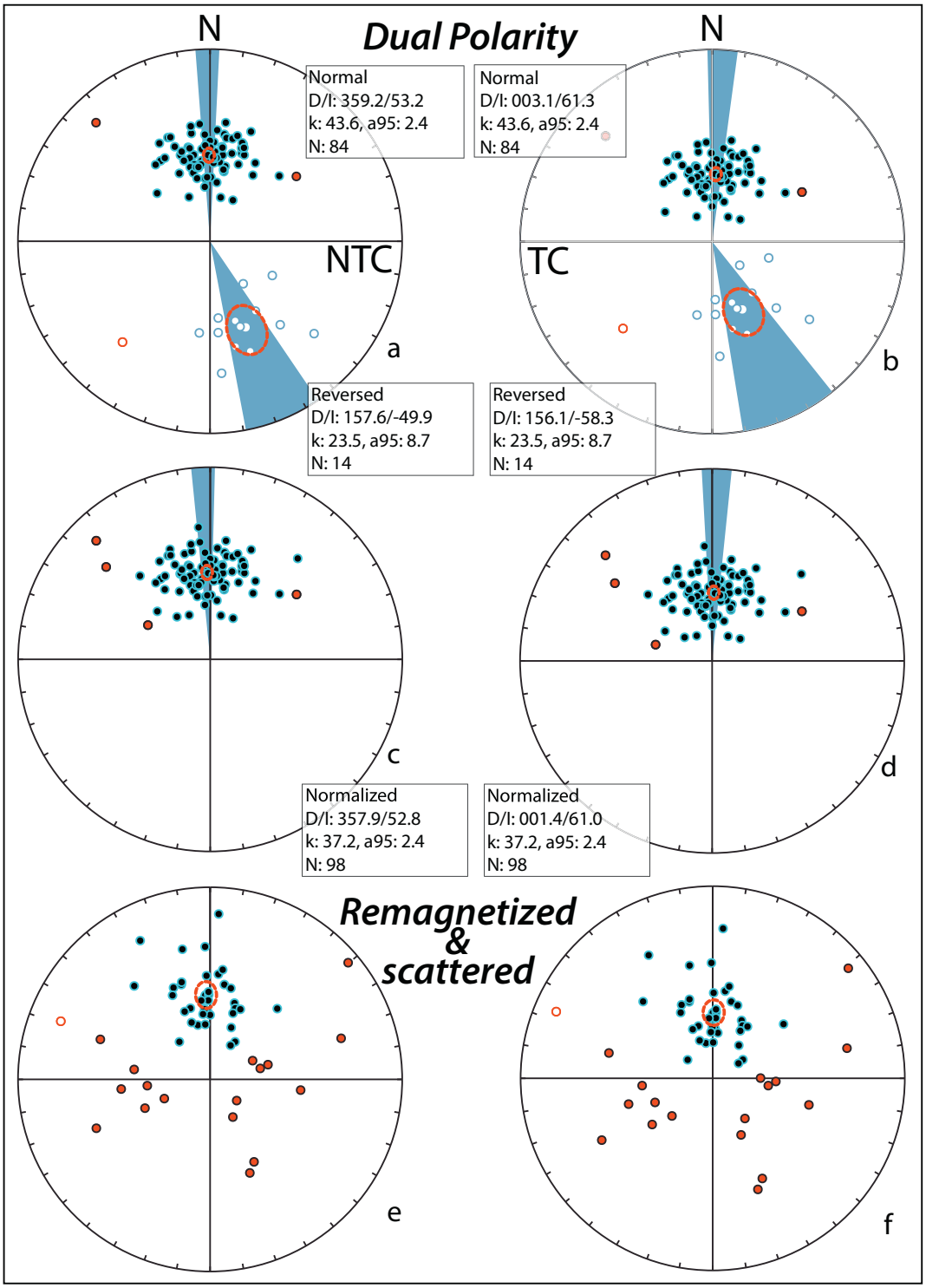

Fig. 8. Equal area projection of both normal and reversed ChRM directions and normalized magnetization results both in situ (NTC) and after tilt correction (TC). Closed (open) symbols indicate projection on lower (upper) hemisphere. Red dashed circles denote mean directions and their cone of confidence (α_{95}). Red solid (open) symbols indicate the individual directions rejected after application of the 45° cut-off. a–d) Reliable results obtained mainly from the upper part of the section starting from 52 m upwards. e–f) Unreliable results mainly from the base of the section. (For interpretation of the references to color in this figure legend, the reader is referred to the web version of this article.)

to be spurious after analysis. The fault slip data were analyzed with the software developed by Delvaux and Sperner (2003). For the analysis, the Rotational Optimization Method (R-Method) was applied, which is based on minimization of the discrepancy between observed (slickensides) and computed maximum shear stress directions by applying various paleostress inversion methods. The resultant directions and statistics are shown in Table 2 and Fig. 10.

In most sites, the angular divergence between computed stress configurations and observed slip-lineations is < 30°. Therefore, each site produced single and relatively consistent stress configurations.

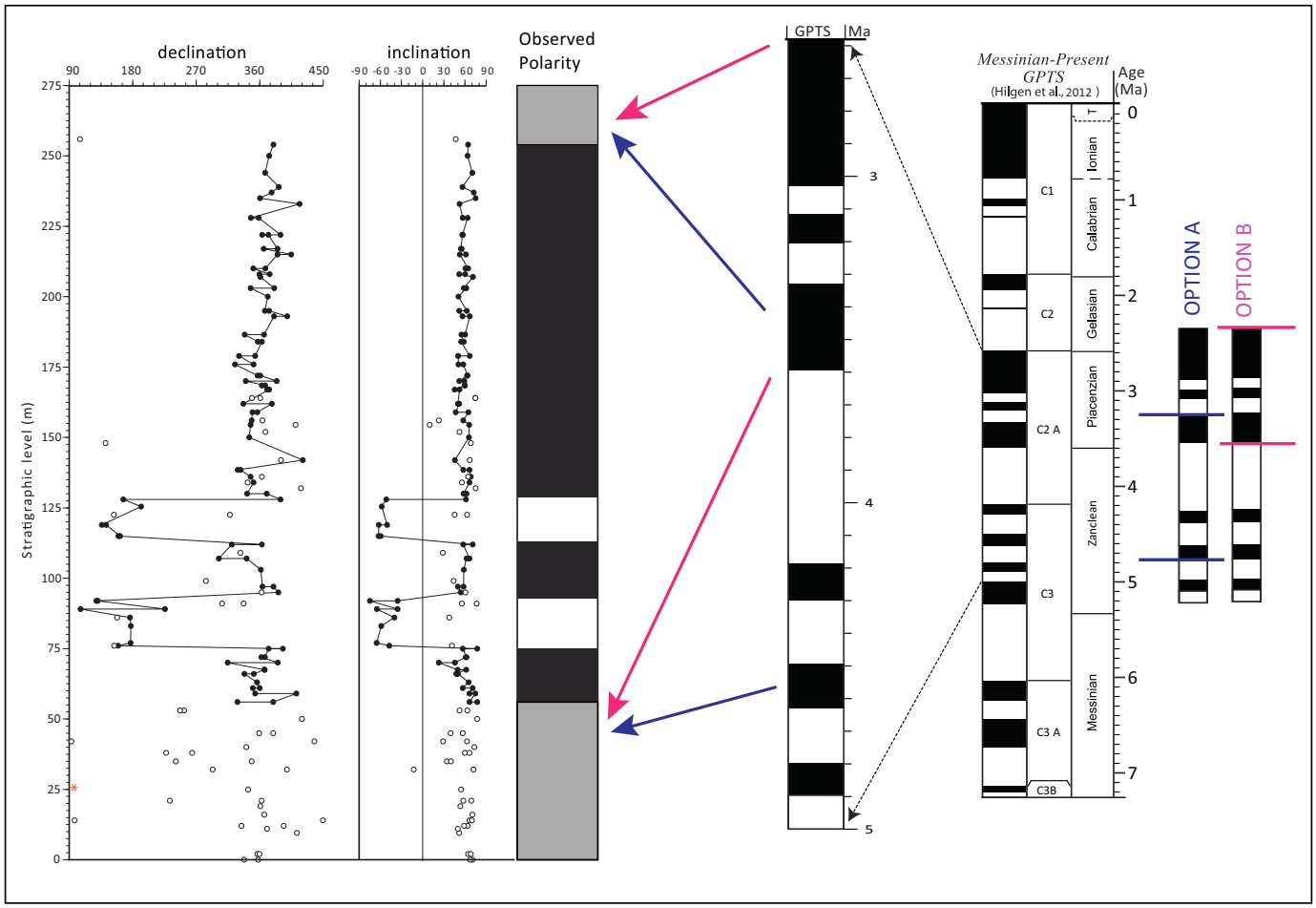

Fig. 9. Magnetostratigraphic correlation of the Burdur section to the GPTS (Hilgen et al., 2012). Normal and reverse polarities are derived from declination and inclination interpretations, where closed points denote reliable and open points denote rejected ChRM directions. The grey points represent unreliable results. In the polarity column, black areas denote normal polarity, white denotes reverse polarity, and grey denote uncertain polarity.

Among the 44 sites, 26 of them indicate approximately NW-SE directed extension while the remaining 18 sites indicate approximately NE-SW directed extension. Almost in all sites, the major stress is near vertical except for sites B18 and B28 where the intermediate stress is sub-vertical. In site FB10, both major and intermediate stress make an angle of around 45° with the vertical, while the minor stress is close to horizontal.

In sites B15, B18, B28 and FB52, the major and the minor stress axes are close to the horizontal while the intermediate stresses axis is sub-vertical; the major stress is trending either E-W or NE-SW, which indicates dextral motion along NE-SW striking faults and sinistral motion along NW-SE striking faults. This is remarkable because among the 44 sites only 6 of the sites indicate strike-slip components and they all collectively imply a dextral component for the faults striking NE-SW, parallel to the longer axes of Burdur and Çameli basins and also parallel to the strike of the Fethiye-Burdur Fault Zone, which is proposed to be sinistral.

6. Discussion

6.1. Origin of the AMS fabric

The AMS technique is capable to determine tectonic deformation even in the absence of any observable strain makers in the field. Since our samples were collected mainly from very fine grained and non-laminated sedimentary levels, it is safe to assume that the AMS tensor is not influenced by sediment transport currents but is only related to post-depositional processes. The general magnetic fabric reveals a mostly sedimentary fabric (compaction) and tectonic influence in its initial stages, with on average a low degree of deformation (Table 1a and Fig. 6). In the Burdur Formation, the magnetic fabric shows a clustering of the lineation (k_1) which represents extension in an ESE-WNW direction, which is almost perpendicular to the main structural trends of ~NE-SW striking normal faults in the basin. This direction is also parallel to the minor stress (s3) orientations near the section (e.g. sites B01, FB9, FB10, FB12 in Fig. 10).

6.2. Depositional age and rate of Burdur Formation

The oldest age of the Burdur Formation is late Miocene based on Girafidae remains reported by Price (1989) found in the alluvial-red beds in the lowest part of the Burdur Formation, close to its southern margin. Recent fossil vertebrate findings encompassing the lacustrine succession (Akdere Member) of the Burdur Formation indicate a Ruscinian age at the base and a Villanyian age at the top of the succession, concurring with previous age determinations (Alçiçek et al., 2013a,b; Alçiçek et al., 2017, 2018). Using this information, the obtained polarity pattern of the Burdur Formation can be correlated to the Geomagnetic Polarity Time Scale (GPTS) of (Hilgen et al., 1995, 2012). Based on biostratigraphical ages the sampled section corresponds to C3 and C2A chronozons (Fig. 9). There are two options for matching the obtained polarity pattern. The oldest age constraint involves taking the sampled tuff layer close to the base of the section into consideration. As mentioned previously, the age of these tuffs – sampled elsewhere –

Table 2
The results of the paleostress analyses (see Fig. 12 for their geographic positions).

SITE	lat	lon	N	σ1 (P/D)	σ2 (P/D)	σ3 (P/D)	Φ
B01	37.69909	30.38112	11	58/305	05/044	32/137	0.52
B04	37.65459	30.16505	32	82/100	05/330	06/239	0.21
B05	37.60597	30.12826	35	55/116	35/300	02/209	0.08
B06	37.58524	30.1145	22	83/015	04/252	06/162	0.31
B07	37.57478	30.11484	6	65/253	09/003	23/097	0.43
B08	37.55738	30.13507	13	55/172	034/336	08/071	0.4
B09	37.57079	30.08853	34	76/085	013/290	06/198	0.08
B10	37.45229	30.05927	47	72/132	03/231	18/322	0.46
B11	37.41028	29.94494	12	74/285	013/065	10/157	0.39
B12	37.3851	29.90268	32	74/272	09/151	14/059	0.46
B13	37.38077	29.86793	32	56/356	30/144	15/243	0.24
B14	37.36296	29.81196	13	69/092	05/196	21/288	0.78
B15	37.17624	29.78923	29	14/103	73/252	08/011	0.5
B16	37.18697	29.64105	18	85/282	03/153	04/063	0.58
B17	37.19699	29.6308	51	72/339	16/179	06/088	0.69
B18	37.19903	29.628	15	33/120	54/273	13/022	0.5
B20	37.16903	29.65847	34	78/263	011/064	03/155	0.68
B21	37.12967	29.50119	37	78/275	00/184	12/094	0.47
B22	37.12698	29.48224	45	78/206	12/028	00/297	0.1
B23	37.11085	29.52172	28	81/293	08/148	05/057	0.17
B24	37.04123	29.46012	21	85/309	03/176	03/086	0.46
B25	37.03216	29.45044	35	79/166	05/284	010/015	0.01
B26	37.03385	29.44551	67	88/338	01/212	02/122	0.2
B27	37.00843	29.39522	27	59/037	31/213	02/304	0.64
B28	36.85985	29.3398	32	04/024	83/256	05/114	0.5
B29	30.115	37.582	7	57/277	12/027	30/124	0.5
FB6	37.92005	30.26962	20	76/013	13/209	04/118	0.07
FB7	37.8967	30.41047	58	76/147	05/033	12/302	0.32
FB8	37.85498	30.49353	28	89/097	00/007	01/277	0.16
FB9	37.73718	30.31129	32	81/028	09/192	03/282	0.1
FB10	37.74283	30.31555	29	43/232	046/037	07/135	0.22
FB11	37.85422	30.42425	49	76/121	10/348	10/256	0.11
FB12	37.6881	30.3477	22	65/241	025/073	05/341	0.28
FB13	37.5993	30.39669	35	64/095	18/323	18/227	0.2
FB14	37.59356	30.4055	43	66/098	24/272	02/003	0.41
FB52	37.27331	29.55862	50	07/050	79/278	08/141	0.52
FB53	37.32218	29.54428	107	77/339	02/240	12/149	0.28
FB54	37.36352	29.49051	67	64/068	25/267	07/173	0.72
FB55	37.52428	29.7349	144	90/030	00/132	00/222	0.64
FB56	37.53231	29.71729	88	79/050	11/232	00/142	0.78
FB57	37.52734	29.72112	81	76/100	13/291	03/200	0.41
FB58	37.5993	29.91824	58	67/321	09/210	21/116	0.44
FB59	37.59457	29.98684	7	82/121	01/022	07/292	0.47
FB60	37.64523	30.04187	137	41/260	48/091	48/091	0.58

D: Direction, P: Plunge, ϕ: Stress ratio, σ1, σ2, σ3: principal stresses (σ1 > σ2 > σ3).

ranges between 4.7 ± 0.2 to 4.0 ± 0.2 Ma (Lefevre et al., 1983). Although the tuff in our section has not been directly dated, this could imply that most of the section is younger than 3.8 Ma, if we include the dating error (Fig. 9). The pattern of the obtained polarity intervals is therefore best correlated to (most of) the Gauss Chron (~3.4–2.5 Ma), although the top of the Gauss is not reliably recorded in the top of the section (grey area with uncertain results) nor the bottom of the Gauss (lower grey area). Hence, presumably we recorded most of the Gauss Chron. With a stratigraphic thickness of at least 200 m, this means that the sedimentation rate is very constant throughout the section, and must be higher than 18 cm/kyr (Fig. 11).

The lithology and the physical properties along the sampled sequence are very similar. There is no apparent evidence that may indicate any significant increase in the sedimentation rate. In addition, there is a rather constant and cyclic pattern (Fig. 4), which – if they were controlled by the known orbital cycles – would suggest a more or less constant accumulation rate. Therefore, a steady sedimentation rate of > 18 cm/kyr is very likely and consistent with our observations.

The Burdur Formation constitutes alluvial, fluvial and lacustrine units as reported by Price (1989) and the paleomagnetic section has been taken from the lacustrine unit (Akdere Member). Therefore it is important to note that, the ~4.0–2.6 Ma time bracket for the lacustrine succession perfectly fits with the vertebrate fossil findings reported by Price (1989) and Alçiçek et al. (2013b, 2017, 2018) from the bottom and the top of that lacustrine succession. We therefore conclude that the lacustrine succession of the Burdur Formation spans the interval from around 4.0 Ma up to 2.6 Ma, i.e. it covers most of the Pliocene.

6.3. Fault kinematics

Most of the faults in the region have a very strong normal character, especially the ones striking NE-SW and hence parallel to the longer axes of Burdur and Çameli basins, which is also parallel to the alleged Fethiye Burdur Shear Zone. Some of the faults have slight strike-slip components, but the sense of the strike-slip components on these faults varies along the fault trace in places. Such fault behaviour is commonly observed as change of the slip vector from pure normal motion at the center of the fault to sinistral and to dextral motion towards the fault tips. The relationship between lateral slip and fault length is approximated by a power-law function such that the strike-slip component is proportional to the dip-slip and to the fault dip (Maniatis and Hampel, 2008).

In addition, some of the NW-SE to E-W striking faults, which are located along the Keçiborlu, Akgöl and Acıpayam transfer zones, also have dextral strike-slip components (Fig. 12). The sense of motion on these faults is very consistent. We argue that these transfer fault zones are developed due to differential stretching between the faults blocks in the region (Fig. 12). These transfer zones are almost perpendicular to the major NE-SW striking normal faults and accommodated dominantly NW-SE directed differential stretching in the region. Having dextral component implies that the fault blocks between the transfer zones are either rotating counter-clockwise or the amount of NW-SE directed stretching of the blocks increases from north to south. In other words, the southern block of each transfer zone has been stretched more than the adjacent northern block.

As seen in Fig. 12a, the major principal stress for almost all sites is oriented subvertical while other stresses are horizontal but unconstrained in any direction. Such an unconstrained orientations of minor stress (σ_3) indicates uniaxial stress conditions. In such tectonic environments, multidirectional extension prevails. Such a configuration is subjected to stress permutation and it commonly develops when the magnitudes of two of the principal stress are equal or close to each other (Angelier and Bergerat, 1983; Hu and Angelier, 2004).

6.4. Temporal relationships

One of the most important issues in paleostress inversion and fault kinematics is related to the determination of deformation phases and their timing. A number of techniques and approaches have already been proposed (e.g. Kleinspehn et al., 1989; Angelier, 1994; Kaymakci et al., 2000). The most reliable method in sedimentary sequences includes dating the faulted strata that is sealing the faulted rocks. This also includes growth faults, which enables construction of paleostress configurations and age of faulted strata. On the other hand, absolute dating of faulting movements include dating of recrystallized and/or authigenic phyllosilicates developed during faulting such as illite (van der Pluijm et al., 2001), and/or organic material using C14 techniques (McCalpin, 2009).

According to Alçiçek et al. (2005, 2006, 2017, van den Hoek Ostende et al., 2015), the age of infill of the Çameli and Burdur basins ranges between late Miocene and Recent, with three major pulses of deposition in the late Miocene, Pliocene and Pleistocene. Our magnetostratigraphic results are in agreement, in that the Burdur Formation was deposited during much or most of the Pliocene.

During the field studies, almost all of the fault slip data were collected from the faults that displace the Burdur Formation or younger units. The main bulk of the data was collected from faults where

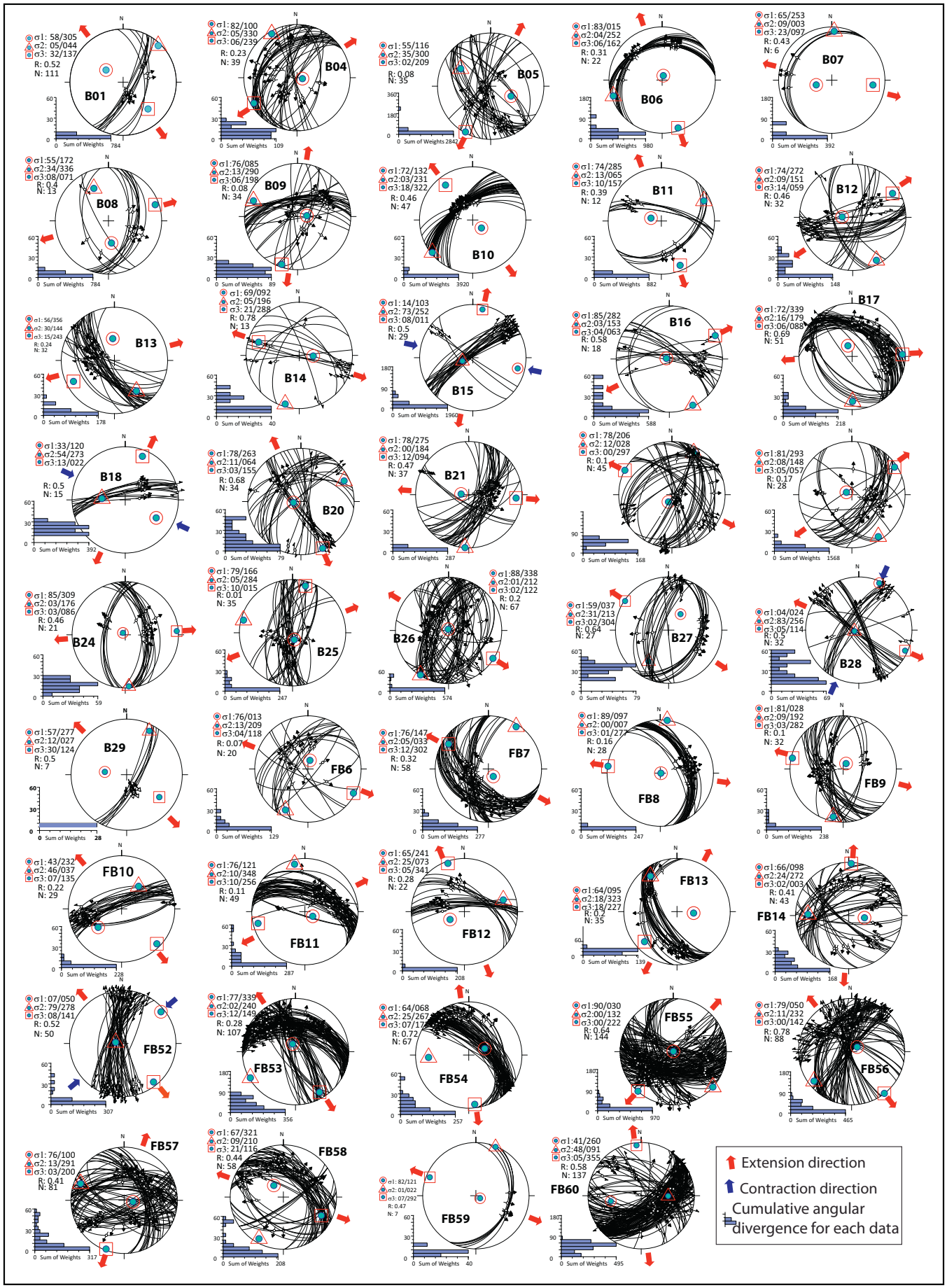

(caption on next page)

Fig. 10. Stereographic projections of constructed paleostress configurations for each site (equal area, lower hemisphere projection) (see Fig. 12 for the locations of sampling sites).

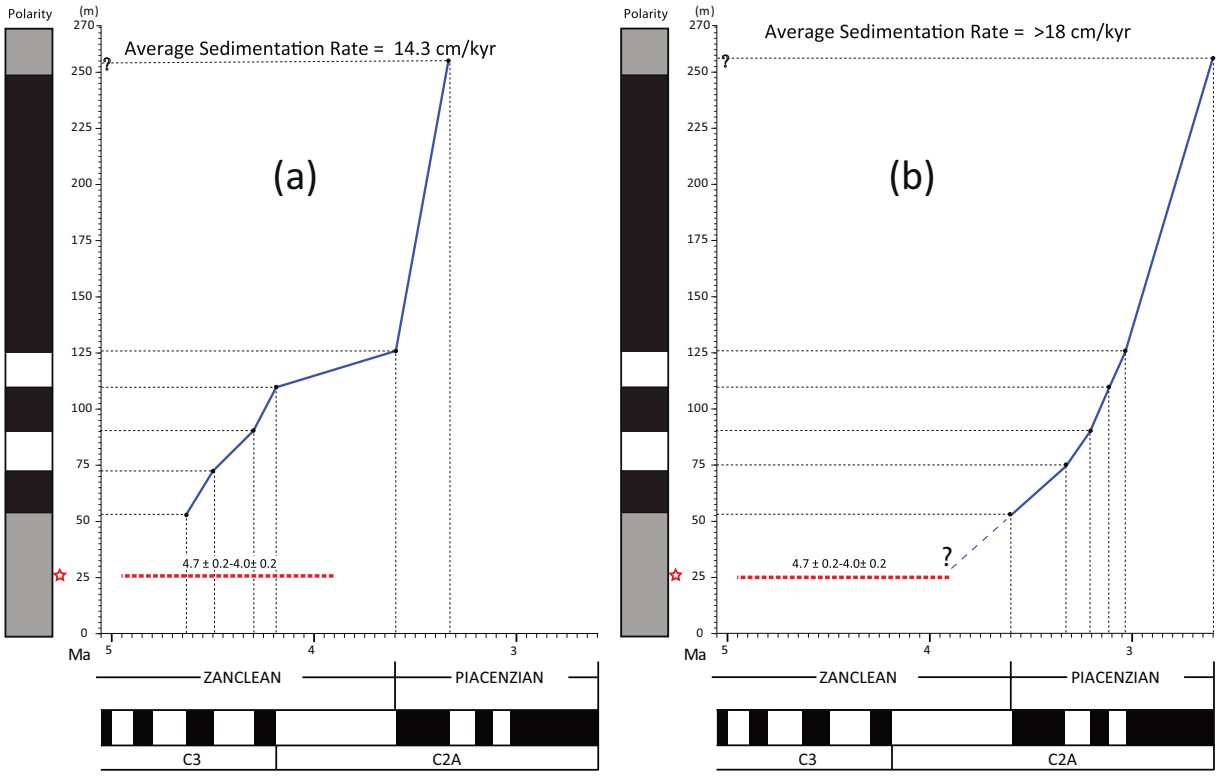

Fig. 11. Age (Ma) versus stratigraphic thickness plots of the Burdur section for two possible correlation options of the magnetozones shown in Fig. 9. a) Sedimentation rate is relatively constant from the base up to ~110 m then it suddenly increase after ~125 m upwards. b) Sedimentation rate is relatively constant from 52 m upwards while it is relatively low at the lower parts. Red dashed line indicates possible age range of sampled tuff layer. (For interpretation of the references to color in this figure legend, the reader is referred to the web version of this article.)

Quaternary alluvial units are abutting fault planes. This implies that most of the faults in the region were active during the Quaternary.

Price and Scott (1991) have demonstrated that the Burdur Basin evolved as an extensional basin since the late Miocene without a break in the intensity and style of deformation. Alçiçek et al. (2005) argued that the Çameli Basin evolved during late Tortonian to Recent times in three phases of extensional deposition, which sequentially deposited younger deposits, while cutting and displacing the older ones. Similarly, Over et al. (2013) argued that the Burdur Basin has been subjected to two phases of extensional deformation during the Pliocene to Recent. Interestingly, Elitez and Yaltırak (2016) – although supporting the existence of the Fethiye Burdur Shear Zone – reported that most of the faults in the Çameli Basin are normal in character and that the region was subjected to extensional deformation, since late Miocene. However, the strike-slip faults reported in Elitez and Yaltırak (2016) are located within the Acıpayam Transfer Zone and are dextral with a reverse component and are striking NW-SE (Site FB52 in Fig. 10).

Considering all the ages and arguments summarized above, we claim that the region of the Çameli and Burdur basins was subjected to extensional deformation since the late Miocene. Current seismic activity and their moment tensor solutions indicate that the same tectonic regime has prevailed in the region since at least early Pliocene to Recent.

6.5. Regional implications

Our magnetostratigraphic results are in agreement with the option that the Burdur Basin developed mainly during the Pliocene, under NW-SE directed extension. The rate of sedimentation was around 18 cm/kyr. The faults are associated with the infill of the Burdur Basin and controlled the deposition in the basin. Some of these faults have been controlling the Quaternary development of the basin, implying that the extensional regime that controlled the region during the Pliocene has continued until recently. Having normal faults in NE-SW direction - rather than sinistral motion along these faults - does not support the presence of a NE-SW striking shear zone. Therefore, we conclude that the existence of a Fethiye-Burdur Shear Zone is not plausible and previously it was not or insufficiently supported by field evidence. Our data clearly indicate that the faults within the presumed Fethiye-Burdur Fault Zone have normal characters, and the region formerly supposed to be dominated by a sinistral strike-slip shear zone is characterized by extensional deformation. Strike-slip motion was encountered only on the faults having NW-SE strikes, which we think correspond to transfer zones that accommodate differential stretching of different domains in SW Anatolia.

7. Conclusions

On the bases of previous fossil assemblages and new magnetostratigraphic data, in combination with field observation, we present new insights into the spatial and temporal evolution of the Burdur Basin. According to the magnetostratigraphy presented in this study the ~270 m thick lacustrine sequence the Burdur Basin is now well dated. This new information indicates that the deposition during the upper Pliocene was almost steady with > 18 cm/kyr sedimentation rate and took place from ~4 Ma to ~2.6 Ma time interval.

The AMS results along the section are conformable with the dominant extension direction in the region, which is oriented in NW-SE direction, perpendicular to the alleged Fethiye Burdur Fault Zone.

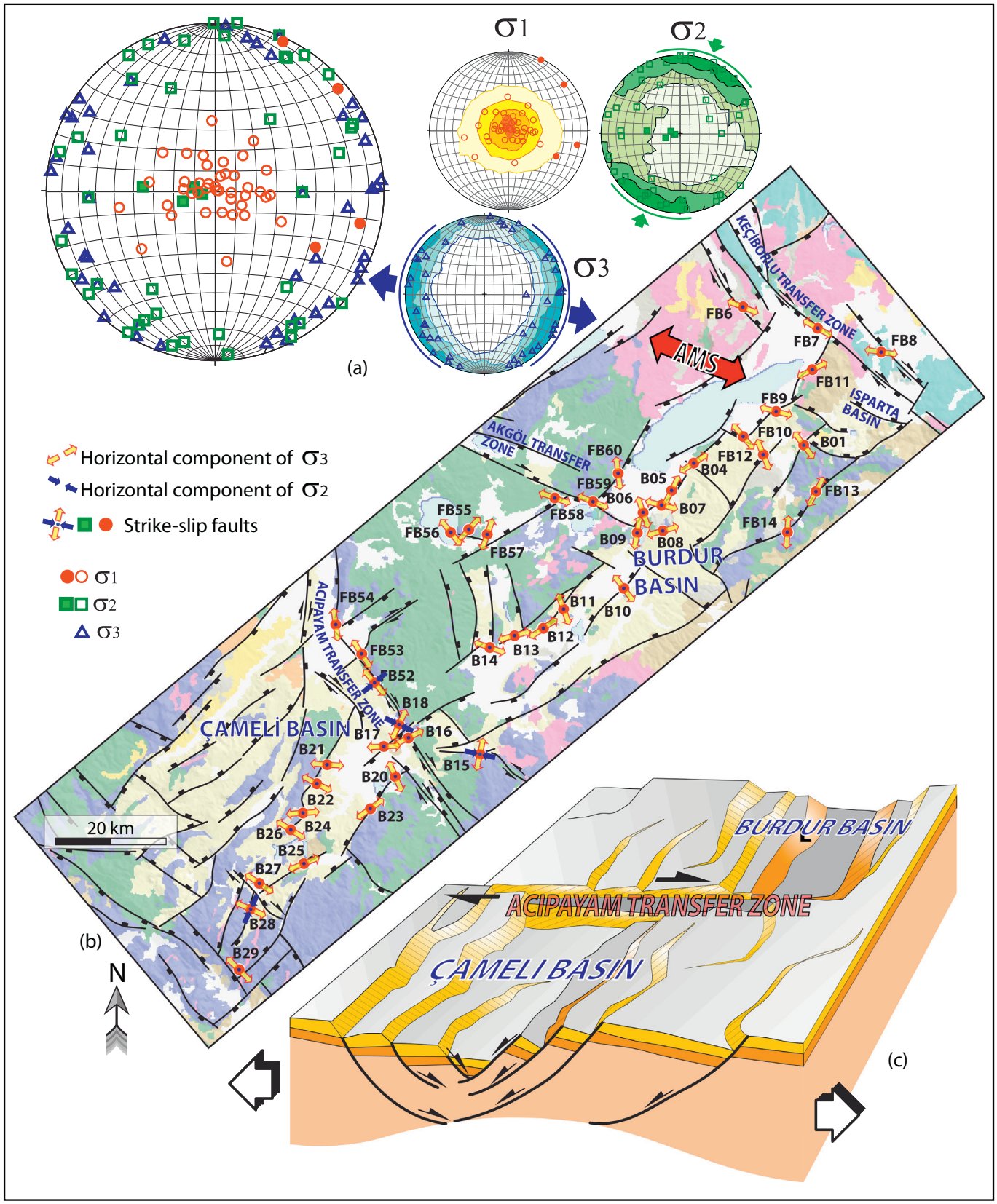

Fig. 12. a) Lower hemisphere, equal area projections of principal stress axes computed for each site. Note that σ_1 is near vertical while σ_2 and σ_3 are subhorizontal except four sites with strike-slip solutions while all other solutions indicate normal faulting. Note also mean WNW-ESE σ_3 and NE-SW σ_2 orientations and scattered patterns of σ_2 and σ_3 implying multi directional extension. b) Simplified tectonic map of Çameli and Burdur basin region along the alleged Fethiye-Burdur Fault Zone. AMS indicates the mean of the k_1 vector. c) Conceptual block diagram depicting extensional transfer fault zone model indicating the relationship between Çameli and Burdur Basins (adopted from van der Pluijm and Marshak, 1997).

Kinematic studies based mainly on fault slip data sets indicated that the basins was subjected to near vertical σ_1, while σ_2 and σ_3 were subhorizontal but not constrained very well in direction, although there is clustering of σ_3 in NW-SE? direction. We interpreted this relationship as multi-directional extension where NW-SE direction dominates. Similar relations were also documented in the Çameli Basin to the south (Alçiçek et al., 2006). We deduced that the multi-directional extension has resulted from similar or nearly equal σ_2 and σ_3 magnitudes. The strike-slip components mainly along the NW-SE striking faults are considered to be caused by the fact that these are transfer faults accommodating differential stretching between fault blocks.

As a conclusion, none of the information obtained in this study does not support the existence of a NE-SW striking transcurrent fault or shear zone that prevailed in the region since the late Miocene. On the contrary, the region was dominated by NW-SE directed extension during this time interval. Therefore, the existence of the Fethiye-Burdur Fault Zone as a surface expression of a STEP fault since the late Miocene cannot be supported.

Plain language summary

We have dated the lacustrine infill of the Burdur Basin to determine its age and rate of deposition. In addition, an extensive kinematic study based on fault slip data sets and Anisotropy of Magnetic Susceptibility measurements have been conducted for better understanding the deformation style and characteristics of the faults in the region. Our results revealed extensional deformation for the Plio-Quaternary and no evidence for the existence of a NE-SW striking sinistral strike-slip fault zone in the region. Thus, our results challenge the presence of the proposed Fethiye-Burdur Fault (or Shear) Zone and on-land continuation of Pliny-Strabo STEP fault in SW Anatolia.

Acknowledgements

Dr. Côme Lefebvre helped during the collection of paleomagnetic samples in 2014. We would like to thank M. Cihat Alçiçek, Douwe van Hinsbergen and two anonymous reviewers for their critical comments, which has improved the paper. This study was supported by the Scientific and Technological Research Council of Turkey [TÜBİTAK, Grant Number 111Y239].

References

Akay, E., Uysal, S., 1988. Post-Eocene tectonics of the Central Taurus Mountains. Miner. Res. Explor. Bull. 108, 23–34. https://doi.org/10.19111/BMRE.86066.

Aksu, A.E., Hall, J., Yaltırak, C., 2005. Miocene to Recent tectonic evolution of the eastern Mediterranean: new pieces of the old Mediterranean puzzle. Mar. Geol. 221, 1–13.

Alçiçek, M.C., 2007. Tectonic development of an orogen-top rift recorded by its terrestrial sedimentation pattern: the Neogene Eşen Basin of southwestern Anatolia, Turkey. Sediment. Geol. 200, 117–140. https://doi.org/10.1016/j.sedgeo.2007.04.003.

Alçiçek, M.C., 2015. Comment on "The Fethiye-Burdur Fault Zone: A component of upper plate extension of the subduction transform edge propagator fault linking Hellenic and Cyprus Arcs, Eastern Mediterranean. Tectonophysics 635, 80–99" by J. Hall, A.E. Aksu, İ. Elitez, C. Yaltırak. Tectonophysics 664, 1–4. https://doi.org/10.1016/j.tecto.2015.01.025.

Alçiçek, M.C., ten Veen, J.H., 2008. The late Early Miocene Acıpayam piggy-back basin: refining the last stages of Lycian nappe emplacement in SW Turkey. Sediment. Geol. 208, 101–113. https://doi.org/10.1016/j.sedgeo.2008.05.003.

Alçiçek, M.C., Kazanci, N., Özkul, M., 2005. Multiple rifting pulses and sedimentation pattern in the Çameli Basin, southwestern Anatolia, Turkey. Sediment. Geol. 173, 409–431. https://doi.org/10.1016/j.sedgeo.2003.12.012.

Alçiçek, M.C., ten Veen, J.H., Özkul, M., 2006. Neotectonic development of the Çameli Basin, southwestern Anatolia, Turkey. In: Robertson, A.H.F., Mountrakis, D. (Eds.), Tectonic Development of the Eastern Mediterranean Region. Geological Society, London, Special Publicationspp. 591–611.

Alçiçek, M.C., Mayda, S., Alçiçek, H., 2012. Faunal and palaeoenvironmental changes in the Çal Basin, SW Anatolia: implications for regional stratigraphic correlation of late Cenozoic basins. Compt. Rendus Geosci. 344, 89–98. https://doi.org/10.1016/j.crte.2012.01.003.

Alçiçek, M.C., Brogi, A., Capezzuoli, E., Liotta, D., Meccheri, M., 2013a. Superimposed basin formation during Neogene-Quaternary extensional tectonics in SW-Anatolia (Turkey): insights from the kinematics of the Dinar Fault Zone. Tectonophysics 608, 713–727. https://doi.org/10.1016/j.tecto.2013.08.008.

Alçiçek, M.C., Mayda, S., Titov, V.V., 2013b. Lower Pleistocene stratigraphy of the Burdur Basin of SW Anatolia. C.R. Palevol 12, 1–11. https://doi.org/10.1016/j.crpv.2012.09.005.

Alçiçek, M., Mayda, S., Demirel, F.A., 2016. Discussion on Neogene-Quaternary evolution of the Tefenni basin on the Fethiye-Burdur fault zone, SW Anatolia-Turkey. J. Afr. Earth Sci. 118, 137–148. https://doi.org/10.1016/j.jafrearsci.2016.07.024. (by R. Aksoy, S. Aksarı).

Alçiçek, H., Wesselingh, F.P., Alçiçek, M.C., Jiménez-Moreno, G., Feijen, F.J., van den Hoek Ostende, L.W., Mayda, S., Tesakov, A.S., 2017. A multiproxy study of the early Pleistocene palaeoenvironmental and palaeoclimatic conditions of an anastomosed fluvial sequence from the Çameli Basin (SW Anatolia, Turkey). Palaeogeogr. Palaeoclimatol. Palaeoecol. 467, 232–252. https://doi.org/10.1016/j.palaeo.2016.08.019.

Alçiçek, M.C., van den Hoek Ostende, L.W., Saraç, G., Tesakov, A.S., Murray, A.M., Hakyemez, H.Y., Göktaş, F., Mayda, S., Jiménez-Moreno, G., Büyükmeriç, Y., Wesselingh, F.P., 2018. Comment on "Miocene to Quaternary tectonostratigraphic evolution of the middle section of the Burdur-Fethiye Shear Zone, south-western Turkey: implications for the wide inter-plate shear zones. Tectonophysics 690, 336–354". Tectonophysics 722, 595–600.

Angelier, J., 1994. Fault slip analysis and paleostress reconstruction. In: Hancock, P.L. (Ed.), Cont. Deform. pp. 53–100.

Angelier, J., Bergerat, F., 1983. Systèmes de contrainte et extension intracontinentale. Bull. Centres Rech. Explor. Prod. Elf-Aquitaine 7, 137–147.

Angelier, J., Lybéris, N., Le Pichon, X., Barrier, E., Huchon, P., 1982. The tectonic development of the Hellenic Arc and the Sea of Crete: a synthesis. Tectonophysics 86. https://doi.org/10.1016/0040-1951(82)90066-X.

Bering, D., 1971. Lithostratigraphie, Entwicklung and Seegeschichte des neogenen und quartären intramontanen Becken der pisidischen Seenregion (Südanatolien). In: Beihefte zum Geol. Jahrb. 101, Hannover.

Biryol, B.C., Beck, S.L., Zandt, G., Özacar, A.A., 2011. Segmented African lithosphere beneath the Anatolian region inferred from teleseismic P-wave tomography. Geophys. J. Int. 184, 1037–1057. https://doi.org/10.1111/j.1365-246X.2010.04910.x.

Borradaile, G., 1987. Anisotropy of magnetic susceptibility: rock composition versus strain. Tectonophysics 138, 327–329. https://doi.org/10.1016/0040-1951(87)90051-5.

Borradaile, G.J., Jackson, M., 2004. Anisotropy of magnetic susceptibility (AMS): magnetic petrofabrics of deformed rocks. Geol. Soc. Lond. Spec. Publ. 238, 299–360. https://doi.org/10.1144/GSL.SP.2004.238.01.18.

Borradaile, G., Tarling, D.H., 1981. The influence of deformation mechanisms on magnetic fabrics in weakly deformed rocks. Tectonophysics 77, 151–168.

Bozcu, M., Yağmurlu, F., Şentürk, M., 2007. Some neotectonic and paleosismological features of the Fethiye-Burdur fault zone, SW-Anatolia. Jeoloji Mühendisliği Dergisi 31, 25–48.

Butler, R.F., 1992. Paleomagnetism: Magnetic Domains to Geologic Terranes. Blackwell Scientific Publications, Boston.

Çemen, İ., Yılmaz, Y., 2017. Part II neotectonics of the Aegean - Western Anatolian Region. In: Eff. Slab-Tear Crustal Struct. Southwest. Anatolia, Act. Glob. Seismol. Neotectonics Earthq. Potential East. Mediterr. Reg. https://doi.org/10.1002/9781118944998.ch4.

Cifelli, F., Mattei, M., Hirt, A.M., Günther, A., 2004a. The origin of tectonic fabrics in "undeformed" clays: the early stages of deformation in extensional sedimentary basins. Geophys. Res. Lett. 31, 2–5. https://doi.org/10.1029/2004GL019609.

Cifelli, F., Rossetti, F., Mattei, M., Hirt, A.M., Funiciello, R., Tortorici, L., 2004b. An AMS, structural and paleomagnetic study of quaternary deformation in eastern Sicily. J. Struct. Geol. 26, 29–46. https://doi.org/10.1016/S0191-8141(03)00092-0.

Cifelli, F., Mattei, M., Chadima, M., Hirt, A.M., Hansen, A., 2005. The origin of tectonic lineation in extensional basins: combined neutron texture and magnetic analyses on "undeformed" clays. Earth Planet. Sci. Lett. 235, 62–78.

Cifelli, F., Rossetti, F., Mattei, M., 2007. The architecture of brittle postorogenic extension: results from an integrated structural and paleomagnetic study in north Calabria (southern Italy). GSA Bull. 119, 221–239.

Çiner, A., Karabıyıkoğlu, M., Monod, O., Deynoux, M., Tuzcu, S., 2008. Late Cenozoic sedimentary evolution of the Antalya Basin, Southern Turkey. Turk. J. Earth Sci. 17, 1–41.

Dankers, P.H.M., Zijderveld, J.D.A., 1981. Alternating field demagnetization of rocks and the problem of gyromagneetic remanence. Earth Planet. Sci. Lett. 53, 89–92.

Deenen, M.H.L., Langereis, C.G., van Hinsbergen, D.J.J., Biggin, A.J., 2011. Geomagnetic secular variation and the statistics of palaeomagnetic directions. Geophys. J. Int. 186, 509–520. https://doi.org/10.1111/j.1365-246X.2011.05050.x.

Deenen, M.H.L., Langereis, C.G., Van Hinsbergen, D.J.J., Biggin, A.J., 2014. Geophys. J. Int. 197 (1), 643.

Delvaux, D., Sperner, B., 2003. Stress tensor inversion from fault kinematic indicators and focal mechanism data: the TENSOR program. In: Nieuwl, D. (Ed.), New Insights Into Struct. Interpret. Model. Geol. Soc. London, Spec. Publ., vol. 212. pp. 75–100.

Duermeijer, C.E., Van Vugt, N., Langereis, C.G., Meulenkamp, J.E., Zachariasse, W.J., 1998. A major late Tortonian rotation phase in the Crotone basin using AMS as tectonic tilt correction and timing of the opening of the Tyrrhenian basin. Tectonophysics 287, 233–249.

Duermeijer, C.E., Nyst, M., Meijer, P.T., Langereis, C.G., Spakman, W., 2000. Neogene evolution of the Aegean arc: paleomagnetic and geodetic evidence for a rapid and young rotation phase. Earth Planet. Sci. Lett. 176, 509–525. https://doi.org/10.1016/S0012-821X(00)00023-6.

Dumont, J.F., Poisson, A., Sahinci, A., 1979. Sur l'existence de coulissements sinistres recentes a l'extermité orientale de l'arc ageen (sud-ouest de la Turquie). CR Acad. Sci.

Paris 289, 261–264.
Elitez, İ., Yaltırak, C., 2016. Miocene to Quaternary tectonostratigraphic evolution of the middle section of the Burdur-Fethiye Shear Zone, south-western Turkey: implications for the wide inter-plate shear zones. Tectonophysics 690, 336–354. https://doi.org/10.1016/j.tecto.2016.10.003.
Elitez, I., Yaltırak, C., 2015. Reply to the comment by MC Alçiçek on "The Fethiye–Burdur Fault Zone: A component of upper plate extension of the subduction transform edge propagator fault linking Hellenic and Cyprus Arcs, Eastern Mediterranean". Tectonophysics 664, 5–13.
Elitez, İ., Yaltırak, C., Aktuğ, B., 2016. Extensional and compressional regime driven left-lateral shear in southwestern Anatolia (eastern Mediterranean): the Burdur-Fethiye Shear Zone. Tectonophysics 688, 26–35. https://doi.org/10.1016/j.tecto.2016.09.024.
Elitez, İ., Yaltırak, C., Kürçer, A., Özdemir, E., Güldoğan, Ç.U., 2017. A critical review of the Kibyra Fault (Burdur-Fethiye Shear Zone, SW Turkey). Geodin. Acta 29, 91–102. https://doi.org/10.1080/09853111.2017.1318001.
Fabian, K., Shcherbakov, V.P., McEnroe, S.A., 2013. Measuring the Curie temperature. Geochem. Geophys. Geosyst. 14, 947–961. https://doi.org/10.1029/2012GC004440.
Faccenna, C., Bellier, O., Martinod, J., Piromallo, C., Regard, V., 2006. Slab detachment beneath eastern Anatolia: a possible cause for the formation of the North Anatolian Fault. Earth Planet. Sci. Lett. 242, 85–97.
Fisher, R.A., 1953. Dispersion on a sphere. Proc. R. Soc. Lond. A 217 (1130), 295–305.
Flecker, R., Ellam, R.M., Müller, C., Poisson, A., Robertson, A.H.F., Turner, J., 1998. Application of Sr isotope stratigraphy and sedimentary analysis to the origin and evolution of the Neogene basins in the Isparta Angle, southern Turkey. Tectonophysics 298, 83–101. https://doi.org/10.1016/S0040-1951(98)00179-6.
Flecker, R., Poisson, A., Robertson, A.H.F., 2005. Facies and palaeogeographic evidence for the Miocene evolution of the Isparta Angle in its regional eastern Mediterranean context. Sediment. Geol. 173, 277–314.
Gong, Z., Dekkers, M.J., Dinarès-Turell, J., Mullender, T.A.T., 2008. Remagnetization mechanism of lower cretaceous rocks from the organyà basin (Pyrenees, Spain). Stud. Geophys. Geod. 52, 187–210. https://doi.org/10.1007/s11200-008-0013-3.
Govers, R., Wortel, M.J.R., 2005. Lithosphere tearing at STEP faults: response to edges of subduction zones. Earth Planet. Sci. Lett. 236, 505–523. https://doi.org/10.1016/j.epsl.2005.03.022.
Graham, J., 1966. Significance of magnetic anisotropy in Appalachian sedimentary rocks. In: Am. Geophys. Union, Geophys. Monogr. Ser.pp. 627–648.
Hall, J., Aksu, A.E., Elitez, I., Yaltirak, C., Çifçi, G., 2014. The Fethiye-Burdur Fault Zone: a component of upper plate extension of the subduction transform edge propagator fault linking Hellenic and Cyprus Arcs, Eastern Mediterranean. Tectonophysics 635, 80–99. https://doi.org/10.1016/j.tecto.2014.05.002.
Hayward, A.B., 1984a. Sedimentation and basin formation related to ophiolite nappe emplacement, Miocene, SW Turkey. Sediment. Geol. 71, 105–129.
Hayward, A.B., 1984b. Miocene clastic sedimentation related to the emplacement of the Lycian Nappes and the Antalya Compex, S.W. Turkey. In: Dixon, J.E., Robertson, A.H.F. (Eds.), Geological Evolution of the Eastern Mediterranean, Geological Society of London Special Publication, pp. 287–300.
Hilgen, F.J., Krijgsman, W., Langereis, C.G., Lourens, L.J., Santarelli, A., Zachariasse, W.J., 1995. Extending the astronomical (polarity) time scale into the Miocene. Earth Planet. Sci. Lett. 136, 495–510.
Hilgen, F.J., Lourens, L.J., Van Dam, J.A., Beu, A.G., Boyes, A.F., Cooper, R.A., Krijgsman, W., Ogg, J.G., Piller, W.E., Wilson, D.S., 2012. The Neogene Period. In: The Geologic Time Scale 2012. Elsevier, pp. 923–978. https://doi.org/10.1016/B978-0-444-59425-9.00029-9.
Hrouda, F., 1982. Magnetic anisotropy of rocks and its application in geology and geophysics. Geophys. Surv. 5, 37–82. https://doi.org/10.1007/BF01450244.
Hu, J.-C., Angelier, J., 2004. Stress permutations: three-dimensional distinct element analysis accounts for a common phenomenon in brittle tectonics. J. Geophys. Res. Solid Earth 109https://doi.org/10.1029/2003JB002616. (n/a-n/a).
Jelínek, V., 1977. The statistical theory of measuring anisotropy of magnetic susceptibility of rocks and its application. Geofizika 22, 50–62.
Jelínek, V., 1978. Statistical processing of magnetic susceptibility measured on groups of specimens. Stud. Geophys. Geod. 22, 50–62.
Jolivet, L., Faccenna, C., Huet, B., Labrousse, L., Le Pourhiet, L., Lacombe, O., Lecomte, E., Burov, E., Denèle, Y., Brun, J.P., Philippon, M., Paul, A., Salaün, G., Karabulut, H., Piromallo, C., Monié, P., Gueydan, F., Okay, A.I., Oberhänsli, R., Pourteau, A., Augier, R., Gadenne, L., Driussi, O., 2013. Aegean tectonics: strain localisation, slab tearing and trench retreat. Tectonophysics 597–598, 1–33. https://doi.org/10.1016/j.tecto.2012.06.011.
Jolivet, L., Menant, A., Sternai, P., Rabillard, A., Arbaret, L., Augier, R., Laurent, V., Beaudoin, A., Grasemann, B., Huet, B., Labrousse, L., Le Pourhiet, L., 2015. The geological signature of a slab tear below the Aegean. Tectonophysics 659, 166–182. https://doi.org/10.1016/j.tecto.2015.08.004.
Karaman, M.E., 1986. General stratigraphy of the Burdur region. J. Akdeniz Univ. Isparta Eng. Fac. 2, 23–36.
Kaymakci, N., White, S.H., Van Dijk, P.M., 2000. Palaeostress inversion in a multiphase deformed area: kinematic and structural evolution of the Çankırı Basin (Central Turkey), part 1–northern area. Geol. Soc. Lond. Spec. Publ. 173, 295–323.
Kaymakci, N., Inceöz, M., Ertepinar, P., Koç, A., 2010. Late Cretaceous to Recent kinematics of SE Anatolia (Turkey). Geol. Soc. Lond. Spec. Publ. 340, 409–435. https://doi.org/10.1144/SP340.18.
Kaymakci, N., Özacar, A.A., Özkaptan, M., Koç, A., Gülyüz, E., Lefebvre, C., Uzel, B., Langereis, C.G., Sözbilir, H., 2014. Fethiye–Burdur fault zone: a myth. In: The 8th International Symposium on Eastern Mediterranean Geology (ISEMG-8), Muğla.
Kaymakci, N., Langereis, C., Özkaptan, M., Özacar, A.A., Gülyüz, E., Uzel, B., Sözbilir, H., 2017. Fethiye-Burdur Fault Zone (SW Turkey): a myth? In: 19th EGU General Assembly, EGU2017. COPERNICUS, Vienna, Austria, pp. 5443.
Kaymakci, N., Langereis, C., Özkaptan, M., Özacar, A.A., Gülyüz, E., Uzel, B., Sözbilir, H., 2018. Paleomagnetic evidence for upper plate response to a STEP fault, SW Anatolia. Earth Planet. Sci. Lett. 498, 101–115. https://doi.org/10.1016/j.epsl.2018.06.022.
Kirschvink, J.L., 1980. The least-squares line and plane and the analysis of palaeomagnetic data. Geophys. J. R. Astron. Soc. 62, 699–718.
Kissel, C., Barrier, E., Laj, C., Lee, T.Q., 1986. Magnetic fabric in 'undeformed' marine clays from compressional zones. Tectonics 5, 769–781.
Kleinspehn, K.L., Pershing, J., Teyssier, C., 1989. Paleostress stratigraphy: a new technique for analyzing tectonic control on sedimentary-basin subsidence. Geology 17, 253–256.
Koç, A., Kaymakci, N., van Hinsbergen, D.J.J., Kuiper, K.F., Vissers, R.L.M., 2012. Tectono-sedimentary evolution and geochronology of the Middle Miocene Altınapa Basin, and implications for the Late Cenozoic uplift history of the Taurides, southern Turkey. Tectonophysics 532, 134–155.
Koç, A., Kaymakci, N., van Hinsbergen, D.J.J., Vissers, R.L.M., 2016a. A Miocene onset of the modern extensional regime in the Isparta Angle: constraints from the Yalvaç Basin (southwest Turkey). Int. J. Earth Sci. 105, 369–398. https://doi.org/10.1007/s00531-014-1100-z.
Koç, A., van Hinsbergen, D.J.J., Kaymakci, N., Langereis, C.G., 2016b. Late Neogene oroclinal bending in the central Taurides: a record of terminal eastward subduction in southern Turkey? Earth Planet. Sci. Lett. 434, 75–90.
Konak, N., Şenel, M., 2002. 1/500.000 Scale Geological Map of Turkey, İzmir Sheet. Ankara.
Koymans, M.R., Langereis, C.G., Pastor-Galán, D., van Hinsbergen, D.J.J., 2016. Paleomagnetism.org: an online multi-platform open source environment for paleomagnetic data analysis. Comput. Geosci. 93, 127–137. https://doi.org/10.1016/j.cageo.2016.05.007.
Le Pichon, X., Angelier, J., 1979. The Hellenic arc and trench system: a key to the neotectonic evolution of the Eastern Mediterranean area. Tectonophysics 60, 1–42.
Lefevre, C., Bellon, H., Poisson, A., 1983. Presence de leucitites dans le volcanisme Pliocene de la region d'Isparta (Taurus occidentales, Turkquie). CR Acad. Sci. Paris 2, 369–372.
Maniatis, G., Hampel, A., 2008. Along-strike variations of the slip direction on normal faults: insights from three-dimensional finite-element models. J. Struct. Geol. 30, 21–28. https://doi.org/10.1016/j.jsg.2007.10.002.
Mattei, M., Sagnotti, L., Faccenna, C., Funiciello, R., 1997. Magnetic fabric of weakly deformed clay-rich sediments in the Italian peninsula: relationship with compressional and extensional tectonics. Tectonophysics 271, 107–122. https://doi.org/10.1016/S0040-1951(96)00244-2.
Mattei, M., Speranza, F., Argentieri, A., Rossetti, F., Sagnotti, L., Funiciello, R., 1999. Extensional tectonics in the Amantea basin (Calabria, Italy): a comparison between structural and magnetic anisotropy data. Tectonophysics 307, 33–49.
McCalpin, J.P., 2009. Application of paleoseismic data to seismic hazard assessment and neotectonic research. Int. Geophys. 95, 1–106.
McFadden, P.L., McElhinny, M.W., 1988. The combined analysis of remagnetisation circles and direct observations in paleomagnetism. Earth Planet. Sci. Lett. 87, 161–172.
Monod, O., Kuzucuoglu, C., Okay, A.I., 2006. A Miocene palaeovalley network in the western Taurus (Turkey). Turk. J. Earth Sci. 15, 1–23.
Mullender, T.A.T., Van Velzen, A.J., Dekkers, M.J., 1993. Continuous drift correction and separate identification of ferrimagnetic and paramagnetic contribution in thermamagnetic runs. Geophys. J. Int. 114, 663–672.
Mullender, T.A.T., Frederichs, T., Hilgenfeldt, C., de Groot, L.V., Fabian, K., Dekkers, M.J., 2016. Automated paleomagnetic and rock magnetic data acquisition with an inline horizontal "'2G"' system. Geochem. Geophys. Geosyst. 17, 2825–2834. https://doi.org/10.1002/2016GC006406.
Nemec, W., Alçiçek, M.C., Özaksoy, V., 2018. Sedimentation in a foreland basin within synorogenic orocline: Palaeogene of the Isparta Bend, Taurides, SW Turkey. Basin Res. 1–21. https://doi.org/10.1111/bre.12269.
Ocakoğlu, N., 2012. Investigation of Fethiye-Marmaris Bay (SW Anatolia): seismic and morphologic evidences from the missing link between the Pliny Trench and the Fethiye-Burdur Fault Zone. Geo-Mar. Lett. 32, 17–28. https://doi.org/10.1007/s00367-011-0234-2.
Over, S., Ozden, S., Yilmaz, H., Pinar, A., Unlugenc, U.C., Kamaci, Z., 2013. Plio-Quaternary stress regime in Eşen Çay Basin, SW Turkey. Geol. Soc. Lond. Spec. Publ. 372, 547–560. https://doi.org/10.1144/sp372.19.
Özbakir, A.D., Şengör, A.M.C., Wortel, M.J.R., Govers, R., 2013. The Pliny-Strabo trench region: a large shear zone resulting from slab tearing. Earth Planet. Sci. Lett. 375, 188–195. https://doi.org/10.1016/j.epsl.2013.05.025.
Özkaptan, M., Koç, A., Lefebvre, C., Gülyüz, E., Uzel, B., Kaymakci, N., Langereis, C.G., Özacar, A.A., Sözbilir, H., 2014. Kinematics of SW Anatolia implications on crustal deformation above slab tear. In: EGU General Assembly Conference Abstracts, pp. 6061.
Passier, H.F., De Lange, G.J., Dekkers, M.J., 2001. Magnetic properties and geochemistry of the active oxidation front and the youngest sapropel in the eastern Mediterranean sea. Geophys. J. Int. 145, 604–614. https://doi.org/10.1046/j.0956-540X.2001.01394.x.
Piper, J.D.A., Gürsoy, H., Tatar, O., Isseven, T., Kocyigit, A., 2002. Palaeomagnetic evidence for the Gondwanian origin of the Taurides and rotation of the Isparta Angle, southern Turkey. Geol. J. 37, 317–336.
Platevoet, B., Scaillet, S., Guillou, H., Blamart, D., Nomade, S., Massault, M., Poisson, A., Elitok, Ö., Özgür, N., Yagmurlu, F., Yilmaz, K., 2008. Pleistocence eruptive chronology of the Gölcük volcano, Isparta Angle, Turkey. Quaternaire 19, 147–156. https://doi.org/10.4000/quaternaire.3092.
Poisson, A., 1984. The extension of the Ionian trough into southwestern Turkey. In: Dixon, J.E., Robertson, A.H.F. (Eds.), The Geological Evolution of the Eastern

Mediterranean. Geological Society, London, Special Publicationpp. 241–250.
Portner, D.E., Delph, J.R., Biryol, C.B., Beck, S.L., Zandt, G., Özacar, A.A., Sandvol, E., Türkelli, N., 2018. Subduction termination through progressive slab deformation across Eastern Mediterranean subduction zones from updated P-wave tomography beneath Anatolia. Geosphere 14 (3), 1–19. https://doi.org/10.1130/GES01617.1.
Price, S., 1989. Sedimentation and Neotectonic of the Burdur Region, SW Turkey (PhD Thesis). Univ. Leicester.
Price, S.P., Scott, B., 1991. Pliocene Burdur Basin, SW Turkey; tectonics, seismicity and sedimentation. J. Geol. Soc. Lond. 148, 345–354.
Price, S.P., Scott, B.C., 1994. Fault-block rotations at the edge of a zone of continental extension, southwest Turkey. J. Struct. Geol. 16, 381–392.
Robertson, A.H.F., Poisson, A., Akinci, Ö., 2003. Developments in research concerning Mesozoic-Tertiary Tetyhs and neotectonics in the Isparta Angle, SW Turkey. Geol. J. 38, 195–234.
Sagnotti, L., Faccenna, C., Funiciello, R., Mattei, M., 1994. Magnetic fabric and structural setting of Plio–Pleistocene clayey units in an extensional regime: the Tyrrhenian margin of central Italy. J. Struct. Geol. 16, 1243–1257.
Scheepers, P.J.J., Langereis, C.G., 1993. Analysis of NRM-directions from the Rossello composite: implications for tectonic rotations of the Caltanisetta basin (Sicily). Earth Planet. Sci. Lett. 119, 243–258.
Şenel, M., 1997. Geological Maps of Turkey at the scale of 1/250.000, Sheets Fethiye and Antalya.
Şenel, M., 2002. 1/500.000 Scale Geological Map of Turkey, İzmir, Ankara, Denizli and Konya Sheets.
Şenel, M., Akdeniz, N., Öztürk, E.M., Özdemir, T., Kadınkız, G., Metin, Y., Öcal, H., Serdaroğlu, M., Örçen, S., 1994. Fethiye (Muğla)-Kalkan (Antalya) ve kuzeyinin jeolojisi. MTA, Rap. Unpubl. 9761.
Şengör, A.M.C., Görür, N., Şaroğlu, F., 1985. Strike-slip faulting and related basin formation in zones of tectonic escape: Turkey as a case study. In: Biddle, K.T., Christie-Blick, N. (Eds.), Strike-slip Deformation, Basin Formation, and Sedimentation. Special Publication Society of Economic Paleontology and Minerology No. 37pp. 227–264.
Soto, R., Casas-Sainz, A.M., Villalaín, J.J., Oliva-Urcia, B., 2007. Mesozoic extension in the Basque-Cantabrian basin (N Spain): contributions from AMS and brittle mesostructures. Tectonophysics 445, 373–394.
Sözbilir, H., 2005. Oligo-Miocene extension in the Lycian orogen: evidence from the Lycian molasse basin, SW Turkey. Geodin. Acta 18, 255–282. https://doi.org/10.3166/ga.18.255-282.
ten Veen, J.H., Boulton, S.J., Alçiçek, M.C., 2009. From palaeotectonics to neotectonics in the Neotethys realm: the importance of kinematic decoupling and inherited structural grain in SW Anatolia (Turkey). Tectonophysics 473, 261–281. https://doi.org/10.1016/j.tecto.2008.09.030.
Üner, S., Özsayin, E., Kutluay, A., Dirik, K., 2015. Polyphase tectonic evolution of the Aksu Basin, Isparta Angle (Southern Turkey). Geol. Carpath. 66, 157–169. https://doi.org/10.1515/geoca-2015-0017.
Uysal, S., Dumont, J.F., Poisson, A., 1980. The Platforms of the Western Taurides. General Directorate of Mineral Research and Exploration, Ankara, Turkey.
Uzel, B., Sözbilir, H., Özkaymak, Ç., Kaymakci, N., Langereis, C.G., 2013. Structural evidence for strike-slip deformation in the İzmir–Balıkesir transfer zone and consequences for late Cenozoic evolution of western Anatolia (Turkey). J. Geodyn. 65, 94–116.
Uzel, B., Langereis, C.G., Kaymakci, N., Sözbilir, H., Özkaymak, Ç., Özkaptan, M., 2015. Paleomagnetic evidence for an inverse rotation history of Western Anatolia during the exhumation of Menderes core complex. Earth Planet. Sci. Lett. 414, 108–125. https://doi.org/10.1016/j.epsl.2015.01.008.
van den Hoek Ostende, L.W., Gardner, J.D., van Bennekom, L., Alçiçek, M.C., Murray, A., Wesselingh, F.P., Alçiçek, H., Tesakov, A., 2015. Ericek, a new Pliocene vertebrate locality in the Çameli Basin (southwestern Anatolia, Turkey). Palaeobiodivers. Palaeoenviron. 95, 305–320. https://doi.org/10.1007/s12549-015-0202-3.
van der Pluijm, B., Marshak, S., 1997. Earth structure: an introduction to structural geology and. Tectonics 673p.
van der Pluijm, B.A., Hall, C.M., Vrolijk, P.J., Pevear, D.R., Covey, M.C., 2001. The dating of shallow faults in the Earth's crust. Nature 412, 172–175. https://doi.org/10.1038/35084053.
van Hinsbergen, D.J.J., Kaymakci, N., Spakman, W., Torsvik, T.H., 2010. Reconciling the geological history of western Turkey with plate circuits and mantle tomography. Earth Planet. Sci. Lett. 297, 674–686.
Van Velzen, A.J., Zijderveld, J.D.A., 1995. Effects of weathering on single domain magnetite in early Pliocene marls. Geophys. J. Int. 267–278.
Verhaert, G., Similox-Tohon, D., Vandycke, S., Sintubin, M., Muchez, P., 2006. Different stress states in the Burdur-Isparta region (SW Turkey) since Late Miocene times: a reflection of a transient stress regime. J. Struct. Geol. 28, 1067–1083. https://doi.org/10.1016/j.jsg.2006.03.013.
Waldron, J.W.F., 1984. Structural history of the Antalya Complex in the 'Isparta angle', Southwest Turkey. In: Dixon, J.E., Robertson, A.H.F. (Eds.), The Geological Evolution of the Eastern Mediterranean. Geological Society, London, Special Publicationpp. 273–278.
Wortel, M.J.R., Spakman, W., 2000. Subduction and slab detachment in the Mediterranean-Carpathian Region. Science 290, 1910–1917. https://doi.org/10.1126/science.290.5498.1910. (80-.).
Yalçınkaya, S., Ergin, A., Afşar, O.P., Taner, K., 1986. Batı Torosların Jeolojisi.
Zijderveld, J.D.A., 1967. A.C. demagnetisation of rocks: analysis of results. In: Collinson, D.W. (Ed.), Methods in Palaeomagnetism. Elsevier, Amsterdam, pp. 254–286.